AD-A133 895

REPORT DOCUMENTATION PAGE		READ INSTRUCTIONS BEFORE COMPLETING FORM
1. REPORT NUMBER AFOSR-TR- 83-0857	2. GOVT ACCESSION NO.	3. RECIPIENT'S CATALOG NUMBER
4. TITLE (and Subtitle) A GENERAL MEASUREMENT DESIGN PHILOSOPHY FOR THE KALMAN FILTER ESTIMATION WITH SPECIAL APPLICATION GIVEN TO THE IMAGING RADAR AUTOFOCUS UPDATE		5. TYPE OF REPORT & PERIOD COVERED FINAL REPORT 01 MAY 1982 to 30 APR 83 6. PERFORMING ORG. REPORT NUMBER
7. AUTHOR(s) William S. McCormick		8. CONTRACT OR GRANT NUMBER(s) AFOSR-82-0127
9. PERFORMING ORGANIZATION NAME AND ADDRESS Wright State University Department of Systems Engineering Dayton, OH 45435		10. PROGRAM ELEMENT, PROJECT, TASK AREA & WORK UNIT NUMBERS 61102F 2305/D9
11. CONTROLLING OFFICE NAME AND ADDRESS Air Force Office of Scientific Research/NE Building #410 Bolling AFB, Washington, DC 20332		12. REPORT DATE 1983 13. NUMBER OF PAGES 60
14. MONITORING AGENCY NAME & ADDRESS(if different from Controlling Office)		15. SECURITY CLASS. (of this report) UNCLASSIFIED 15a. DECLASSIFICATION/DOWNGRADING SCHEDULE

16. DISTRIBUTION STATEMENT (of this Report)

Approved for public release;
distribution unlimited.

17. DISTRIBUTION STATEMENT (of the abstract entered in Block 20 if different from Report)

18. SUPPLEMENTARY NOTES

DTIC
ELECTE
OCT 2 1983
E

19. KEY WORDS (Continue on reverse side if necessary and identify by block number)

20. ABSTRACT (Continue on reverse side if necessary and identify by block number)

The value of an Autofocus update of an INS is investigated. Three cases are considered: (1) centripedal acceleration only; (2) centripedal and line-of-sight acceleration; and (3) centripedal and line-of-sight acceleration as well as attitude error effects. The extended Kalman filter configuration was employed using the versatile SOFE Monte Carlo simulation program. Measurement matrices were defined for each of the three cases. Simulation results indicated an observability problem for Case (1). Suggestion for further work

DD FORM 1 JAN 73 1473 EDITION OF 1 NOV 65 IS OBSOLETE

UNCLASSIFIED

SECURITY CLASSIFICATION OF THIS PAGE (When Data Entered)

DTIC FILE COPY

was included. For the centripedal acceleration case only, the Autofocus measurement proved to be a useful measurement when supplemented by additional measurements. In particular, a Compass, an Autofocus, and doppler velocity update realize better than a 94% update quality. Without the Autofocus, the quality suffers greatly.

MINI-GRANT

FINAL REPORT

"A General Measurement Design Philosophy For the Kalman Filter Estimation With Special Application Given to the Imaging Radar Autofocus Update"

Author: William S. McCormick
University: Wright State University, Dayton, Ohio
Department: Engineering
Sponsoring Agency: AFOSR-82-0127

I. Introduction

Much of the summer project (1981) period was devoted to an understanding of the extended Kalman filter and to how the Autofocus measurement could be implemented using the versatile Monte Carlo simulation program called SOFE.[1] Using the 45th order dynamics of a Honeywell LN-15 local-level INS truth model, a 13th order approximating filter was chosen and a linearized Autofocus measurement matrix derived. With a typical "climbing" trajectory generated by the program PROFGEN, the system was run over various sections of aircraft trajectory at high measurement S/N ratios and without any additional scaler measurements used to supplement the Autofocus measurement. Generally, the update quality of the Autofocus measurement was disappointing with a good initial update being followed invariably by a confused, "wandering" update. (Appendix A includes the entire summer project final report for background information). Since the observability matrix of the system was determined to be singular, it was concluded (by default) that the nonobservability of the system when coupled with the high measurement S/N ratio was perhaps introducing a significant roundoff error instability into the update mechanism and was therefore the source of the poor performance. This instability phenomenom has been frequently reported in the literature but it was a somewhat unsatisfying explanation since roundoff problems do not usually occur on the WPAFB CYBER 64 bit machine. Furthermore, little problem was experienced with either filter divergence or with the covariance matrix converging to a nonpositive definite steady-state solution. In short, the alleged nonobservability effect was a questionable explanation

but it was the most plausible one available. The only other possible explanation was that the Autofocus measurement was simply too ambiguous or too loosely coupled to the state vector to be a useful scaler measurement. However, this last explanation was not consistent with the uniformly good initial updates achieved.

II. Description of Computer Runs Performed in Summer of 1982

A. General Remarks

The system as of 6/30/82 included only the Autofocus measurement in the centripedal acceleration mode. The trajectory used was the original trajectory tape of the summer of 1981 which featured a slow climb and leveling out manuever. During the spring of 1983, the line of sight (L.O.S) acceleration term was added to the measurement. All measurements in the project were high S/N measurements and were simulated as such. Error feedback after update was used until 10/83. Error feedback created a subtle problem in evaluating the quality of the update and was also thought to have generated an error propagation path. Process noise was added to the covariance propagation model in order to control filter divergence. The observed update performance did not seem to be sensitive to the magnitude of the process noise in most instances although filter divergence occurred if no noise was added.

B. Check for Algebraic Sign Error and Preliminary Runs

A common problem in Kalman filter simulation work is the occurrence of simple algebraic sign errors in the measurement simulation (HRZ subroutine in SOFE) section. In order to gain confidence

that a good update was even possible with the truth model used, 13 separate measurements were postulated at high S/N ratios for each of the 13 filter state variables. Excellent updates were observed along with strong covariance updates; with confidence in the simulation implementation acquired, various combination of state variables were measured independently with or without the Autofocus measurement. It was observed that while the Autofocus provided some useful update information by itself, it did benefit greatly from a supplementary measurement on the velocity vector. It was also observed that latitude and longitude updated well when each velocity component was measured independently. This was not surprising since latitude and longitude are position variables which are strongly coupled to the velocity vector.

C. <u>The PBH Test for Observability; The Eigenvalue/vector of P_f Matrix; and Elimination of the Error Feedback Mode</u>

In the 8/82 to 9/82 period, a number of useful steps were taken to resolve the observability question. During the summer of 1981, the observability matrix was programmed in the user routine, ESTIX; the determinant of the matrix was formed and found to be zero for all runs which indicated a nonobservable system. This fact alone provides little information since any nonobservable state variable will cause a zero determinant even if it is too loosely coupled to the system to have any real effect on system performance. Condition numbers can of course be defined on the matrix eigenvalues but these indexes are misleading and are usually sensitive to the wrong factors. In the present

investigation, the PBH test was used to investigate nonobservability. Briefly stated, the PBH test indicates the nonobservability of a system if and only if there exists an eigenvector of the system matrix, A that is orthogonal to the measurement vector. (The proof is available in Kailath[2]). Accordingly, the eigenvectors of the system matrix were generated in ESTIX by using the IMSL routine EIGRF and then used to form a generalized inner product with the measurement vector. In order to portray the "degree" of orthogonality or observability, a generalized cos(θ) was then formed over the complex field as

$$\cos_k(\theta) = \frac{\left| \sum_{i=1}^{n} a_k^i H_i \right|}{\sum_{i=1}^{n} |a_k^i| \cdot \sum_{i=1}^{n} |H_i|^{\frac{1}{2}}} \qquad (1)$$

where a_k^i is the i^{th} component (in general complex) of the k^{th} eigenvector of A and H_i in the i^{th} component of the measurement vector. For the Autofocus only measurement, the above measure was ≈ 0 for 7 of the 13 variables and was around 0.6 for the other 6 variables. Since simulation runs indicate significant updates only for the position and velocity variables, it can be concluded that these variables are the only strongly observable ones and that the seven other variables (attitude, bias, and gyro drift states) are only weakly observable with the centripedal-only Autofocus measurement. It is interesting to speculate that the measure, cos(θ), may indicate the degree of measurement observability which would then reflect either the number of updates required for a given measurement to update the state vector or the sensitivity of the state vector update quality to measurement

noise. As support for the significance of the magnitude of cos(θ), the Autofocus measurement with the L.O.S. term has 9 observable variables but no cos(θ) exceeds the value of 0.2, and the measurement does not update as well for the same number of updates as the centripedal only case.

The error feedback was also discontinued in 10/82 and the error of update defined as

$$\text{update error} = \frac{|XS(i)-XF(i)|}{|XS(i)|} \times 100\% \qquad (2)$$

was calculated and printed out in ESTIX.

D. Resolution of Observability Question

As of 11/82, the identity of the weakly observable state variables was known. It remained to determine what effect, if any, they had on the mediocre Autofocus update. The definite test was taken by removing the "nonobservable" variables from the filter and then observing the update quality. This procedure was performed by setting the appropriate filter model derivatives to zero. No significant degradation in the Autofocus update was observed which led to the conclusion that at least for the Autofocus measurement alone, no significant effect due to nonobservability is present. This does not mean that that the altitude/drift variables can not be updated. They can be updated especially with additional measurements but the update is a slow one due to the very low value of $\cos(\theta_k)$. This slow update situation can also be explained by the near orthoganality of

the measurement vector and the eigenvectors of P_f associated with the poorly observable states. More will be said on this in a later section.

In conclusion, the observability problem does not appear to be the cause of the mediocre Autofocus update. It should be noted that the same result could be revealed from matrix partitioning as well.

It should be acknowledged that the PBH test applies only to the time invariant systems as do the usual tests on the observability matrix. In a time varying system, as considered in this project, the usual measure of observability must be modified slightly. Nevertheless, the $\cos(\theta_k)$ can be a useful indicator of the type of coupling that exists between measurement and state vectors.

E. The Introduction of Additional Measurements

Referring to Table B1, of Appendix B, an Autofocus measurement alone is presented for t>0 with a time between updates of 8 sec. and a time delay before the first update of 48 secs. Through 20 updates, the update error measurements, in percentages, for the first six state variables are (64, 43, 114, 61, 22, 115) respectively. It is apparent that the scaler Autofocus measurement needs an additional measurement to improve the update quality. Considering the Autofocus value measurement as a plane in state error space defined by

$$\begin{matrix}\text{Autofocus} \\ \text{Measurement}\end{matrix} = K\, H_4 \delta V_E + H_5 \delta V_N + H_6 \delta V_Z \qquad (3)$$

where H_4, H_5, H_6 are components of the measurement vector and the (δV_E, δV_N, δV_Z) are components of the velocity error vector, we can

consider the first update as the optimum update given the position of the measurement plane relative to the covariance ellipsoid. Depending on the relative positioning of the plane and ellipsoid, the state error vector will be restricted to a certain defined region of state error space which represents the geometrically underdetermined nature of the measurement. Repeated Autofocus measurements will cause the error vector to wander about this region due to the influence of unmodeled state variables. Any additional scaler measurement should reduce the "volume" of this region of uncertainty and therefore improve the reliability of the update.

F. The Introduction of The Compass Measurement

A logical supplementary measurement is a Compass measurement which measures heading, θ, given in terms of the east and north velocity, V_E, V_N, components as

$$\theta = \tan^{-1} \frac{V_E}{V_N} \tag{4}$$

which yields a measurement matrix row entry of $H_4 = \frac{V_N}{1+(V_E)^2}$ and $H_5 = \frac{-V_E}{1+(V_E)^2}$ and which also introduces a new measurement plane defined by

Compass measurement $= H_4 \delta V_E + H_5 \delta V_N$, that further restricts the volume of in the state vector error ellipsoid. Indeed, the Autofocus and Compass measurement would determine the velocity state-error vector uniquely were it not for the dependence of the Autofocus on the unknown vertical velocity component. Accordingly, it would be reasonable to expect

the best updates to occur in level flight where $V_Z \approx 0$. However, this is exactly the opposite of what actually occurred. For the level flight period around t = 16 minutes, the update became quite shaky for the simple reason that the Autofocus and Compass measurement planes began to approach a parallel state in which their region of intersection became very sensitive to unmodeled state variables in the measurement process. This phenomena only illustrates the complexity and surprises that await the investigator.

The degree of improvement for the Autofocus/Compass combination for the $t \geq 0$ slow climb trajectory interval can be expressed, as in section E, by the 6 mean percentage values of the first six variables given as (11, 11, 115, 21, 16, 116) in Table B2. Despite the unknown V_Z component, the Compass measurement significantly improves the update because its measurement plane in this particular flight interval is nearly at right angles to the Autofocus measurement plane and the region of intersection is less sensitive to the unmodeled truth state variables. The value of the Autofocus measurement in this two measurement scheme can be appreciated by the increase in velocity error vector in Table B3 to (34%, 141%, 100%) when the Compass measurement alone is used. This is to be contrasted to the (11%, 11%, 115%) velocity error for the Autofocus/Compass combination.

G. The Addition of Doppler Vertical Velocity and Altimeter Measurements

With the value of supplementary measurements established, a doppler vertical velocity measurement was added in order to remove the uncertainty in the last remaining velocity component. A significantly improved update was obtained with the percentage means of the first six variables given in Table B4 as (5.46, 7.0, 35, 17, 11, 2) which represents a 50% improvement in the position variables, a 70% improvement in altitude, and finally a 33% improvement in V_E and V_N estimation.

V_E and V_N estimation.

An additional altitude measurement was added to the update but, as indicated in Table B5, it affected only the altitude variable itself.

H. A Definitive Statement of the Value of the Autofocus Measurement in the Centripedal Model

At this point in the report, it is possible to evaluate the true value of the Autofocus measurement - one of the primary objectives of the original investigation. The evaluation will be made by contrasting the mean and standard deviation of the update error for the six observable states over at least 20 updates in both the three and four measurements cases. The following Tables H(a) and (b) condense the detailed data available in Appendix B in Tables B4, B7, B6, and B13

Without Autofocus (%)		With Autofocus (%)	
State	(m;σ)	State	(m;σ)
1	(45;7.7)	1	(5.46;3.66)
2	(153;25)	2	(7.0;6.81)
3	(58;20)	3	(35;27)
4	(51;25)	4	(17;14)
5	(134;26)	5	(11;12)
6	(1.10;0.54)	6	(1.10;0.54)

Table H(a): Three Measurement Case (Tables B4 and B7)

Without Autofocus (%)		With Autofocus (%)	
State	(π,σ)	State	(m,σ)
1	(44;4.2)	1	(7.14;3.41)
2	(161;19.2)	2	(7.66;2.76)
3	(2.74;2.74)	3	(3.34; 2.57)
4	(56;24)	4	(17.5;15.9)
5	132;32)	5	(11.4;12.5)
6	2.;0.74)	6	(3.3;3.64)

Table H(b): Four Measurement Case (Tables B6 and B13)

It is clear from Table H(a) and (b) that the Autofocus (centripedal) measurement is a useful high S/N measurement and should be considered operationally provided it is supplemented by other measurements.

I. The Effect of Varying Measurement Time

The time between updates was determined largely by the aperture times of the imaging radar Autofocus measurement. Typically, these times can range anywhere from 1 to 20 seconds in length with 8 sec. being used for the great majority of runs in this project.

In order to investigate the sensitivity of update accuracy to aperture time, a number of runs were made at update intervals of 4 and 16 seconds respectively. Referring to Tables B8 and B9, the mean value of the respective velocity component error are (12, 10, 1.12) and (18, 12, 1.09) for the 4 and 16 second three measurement case respectively. It is apparent the system dynamics is highly correlated over a 20 sec. interval and that little independent information is added at the higher update rate.

III. New Results

A. General Remarks

Because the measurements considered in this work were uniformly high S/N ratio measurements, it was natural to consider the state-error vector as a point contained to an n-dimensional plane defined by the following equation,

$$(\text{Measurement}) = \vec{H} \cdot \vec{\delta X} = h_1 \delta x_1 + h_2 \delta x_2 + \cdots + h_N \delta x_N \qquad (5)$$

with $\vec{H} = [h_1, h_2, \cdots, h_N]$ equalling the measurement vector or single-row matrix. This interpretation of the scaler measurement led naturally to a geometrical interpretation of the entire system update mechanism. In particular, the propagating covariance matrix, P_f, was diagonalized by the IMSL routine, EIGRF, and the eigenvalues/eigenvectors of P_f printed out. Using the concepts of principal component analysis in multivariate statistics, the eigenvalues were interpreted as levels of uncertainty associated with a particular eigenvector direction. Geometrically, the diagonalization defines an n-dimension error ellipsoid, whose relative orientation with respect to the measurement vector, H, will completely define the nature and value of the update. The interpretation of the update as an orienting of the measurement plane with respect to the covariance ellipsoid will constitute the remainder of this section.

B. Diagonalization P_f and the Forming of cos(θ) Between $\vec{H}$ and the P_f Eigenvectors

The covariance matrix P_f was, from the beginning, a routine printout in the SOFE extended kalman filter simulation. Not a

great deal of attention was paid to P_f until the supplementary measurements were added to the basic Autofocus measurement around January of 1983. Because of the noticeable improvement when additional measurements were added, the covariance matrix, P_f, was printed out after each of the M measurements instead of simply at the end of the complete update as before. Unfortunately, the P_f matrix as a full matrix, is difficult to interpret; therefore the correlation matrix was also formed and printed out. However, the correlation matrix, although normalized, is still a full matrix and does not clearly portray the independencies or cross correlations between the state-variables. It was at this point that the decision to diagonalize P_f was made. It was the result both of the experience gained with the EIGRF routine and also from the image compression background of the author wherein the K-L or karhuen-Loeve transformation is routinely used to compress images. It was later discovered that the diagonalization of P_f approach was really equivalent to the principal component approach in multivariate statistics which had been developed some twenty years ago by Pearson and Hotelling. Briefly stated, the diagonalization of the real symmetric matrix, P_f, produces real eigenvalues along with a set of orthogonal eigenvectors with real components. Each eigenvalue represents the variance or uncertainty associated with the direction of its particular eigenvector. The sum of the eigenvalues will represent the total variance or uncertainty of the filter model at some point in the update. One very significant advantage of the diagonalization lies in the ability to associate levels of variance or uncertainty with certain state variables by simply observing their normalized component values in those eigenvectors associated with the significant eigenvalues.

From equation (5), the measurement plane can be interpreted as a plane perpendicular to the measurement vector defined as (h_1, h_2, 0, 0, 0, h_n). Intuitively, it would seem that the Kalman update would attempt to make the P_f eigenvectors lie within the measurement plane after update in order to ensure that a particular scaler measurement could contribute (or project) no further information to the filter. Such a geometric condition can be expressed succinctly as $H \cdot P_k = 0$; $k = 1, 2, \cdots, n$ where P_k is the k^{th} eigenvector of P_f, the P_f before update. Gelb[3] illustrates the geometric interpretation or the updates for the simple two state case shown in Figure 1. In this case, the measurement of $\hat{y}_1$ intersects the eigenvector or major axis of the covariance ellipse to give a projected or estimated value of x_1'. The covariance of the ellipse provides the correlation or best linear estimate of x_1 by using the correlation between x_1 and y_1 to reduce to state-error variables from two to one thereby reducing the overall measurement to a completely determined problem. Considering the measurement, $\hat{y}_1$, as z, the best estimate $\hat{x}_1'$, is equal to $z \tan(\theta)$ or $z \frac{\sin(\theta)}{\cos(\theta)}$. In this case, the measurement matrix equals (1,0) since y is $y = z =$ constant and is perpendicular to the y - axis; it follows that $\lambda_1(H \cdot P_1) = \lambda_1 \cos(\theta)$ and $\lambda_1 P_1^{(x)} = \lambda_1 \sin(\theta)$ where $\lambda_1 P_1^{(x)}$ is the x-axis projection of the normalized P_1 vector which then suggests the following expression for $\hat{x}_1$;

$$\hat{x}_1' = z \frac{\lambda_1 P_1^{(x)}}{\lambda_1 (P_1 \cdot H)} = \frac{z\, P_1^{(x)}}{(P_1 \cdot H)} = z \frac{\sin(\theta)}{\cos(\theta)} = z \tan(\theta) \qquad (6)$$

as before.

Because of the intuitive appeal of the $(H \cdot P_k)$ value, the cosine of the angle or $\frac{(H \cdot P_k)}{\sqrt{|H| \cdot |P_k|}}$ was printed out for $k = 1,2,3, \cdots, n$. As

expected, the update tended to drive all $(H \cdot P_k)$ to zero as has, in fact, been confirmed by every simulation run. This is by itself a useful result that will be used to define practical indexes of measurement performance in Section D.

The next section will restate the Kalman update equations in terms of the eigenvalues/eigenvectors of P_f. The series of derivations will reinforce the significance of the $(H \cdot P_f)$ measure and will represent the key analytical result of the project.

D. The Kalman Update Equation Expressed in Terms of the Eigenvalues/Eigenvectors of P_f

1. General Remarks

In this section, the Kalman update equations will be restated in terms of the eigenvalue/eigenvector of the covariance matrix before update. The notation will represent quantities before update with the superscript - and quantities after update with the superscript +. The update equation considered are the following:

a. State Error Vector Update

$$\underline{X}_f^+ = \underline{X}_f^- + K(Z - H\underline{X}_f^-)$$

where the essential gain vector, K, is given as

$$K = P_f^- H^T(HP_f^-H^T+R_f)^{-1} \tag{7}$$

where R_f is the measurement noise variance taken to be zero under the high S/N assumption.

b. Covariance Update

$$P_f^+ = P_f^- - KHP_f^- \tag{8}$$

In the following derivations, the quantities are usually defined before the update and will not therefore carry the - superscript. The eigenvalues will be designated as λ_n; n = 1,2,··· and the corresponding eigenvectors as $\underline{P}_n$ with the k^{th} component of the n^{th} eigenvector represented by P_n^k.

2. The Common Denominator Term: $(HP_f H^T)^{-1}$

In terms of λ and $\underline{P}$, the high S/N denominator term can be expressed as

$$\text{Denom. Term} = [H]\left\{[\underline{P}][\lambda][\underline{P}]^T\right\}[H]^T \tag{9}$$

or, upon matrix multiplication,

$$\text{Denom. Term} = [\underline{P}_1 \cdot H, \underline{P}_2 \cdot H, \cdots, \underline{P}_n H][\lambda]\begin{bmatrix} \underline{P}_1 \cdot H \\ P_2 \cdot H \\ \cdot \\ \cdot \\ \underline{P}_n \cdot H \end{bmatrix} \tag{10}$$

which becomes,

$$\text{Denom. Term} = [\underline{P}_1 \cdot H, P_2 \cdot H, \cdots, P_n \cdot H]\begin{bmatrix} \lambda_1(\underline{P}_1 \cdot H) \\ \lambda_2(\underline{P}_2 \cdot H) \\ \cdot \\ \cdot \\ \cdot \\ \lambda_n(\underline{P}_n \cdot H) \end{bmatrix}, \tag{11}$$

and then finally

$$\text{Denom. Term} = \sum_{k=1}^{n} \lambda_k (\underline{P}_k \cdot H)^2 \tag{12}$$

which is an important result.

3. The Covariance Update

From the second distributive law of matrix multiplication, $P_f^+ = P_f^- - KHP_f^-$ can be expressed as $P_f^+ = (I-KH)P_f^-$ where I is the identity matrix. One measure of a good update is the decrease of the (i,i) entry of the P_f^+ matrix or, equivalently, the degree to which $(KH)_{ii}$ approaches I. It is therefore the product, KH, that is of interest and which can be expressed as

$$KH = \frac{P_f H^T H}{\sum_{k=i}^{n} \lambda_k (\underline{P}_k \cdot H)^2} \tag{13}$$

The term, $P_f H^T H$, can be written in terms of $\lambda_i, \underline{P}_i$ as

$$P_f H^T H = [\underline{P}][\lambda][\underline{P}]' \begin{bmatrix} h_1 \\ h_2 \\ \cdot \\ \cdot \\ \cdot \\ h_n \end{bmatrix} [h_1, h_2, \cdots h_n] \tag{14}$$

which, after additional multiplication, becomes

$$P_f H^T H = \begin{bmatrix} \lambda_1 P_1^1, \lambda_2 P_2^1, \cdots, \lambda_n P_n^1 \\ \lambda_1 P_1^2, \lambda_2 P_2^2, \cdots, \lambda_n P_n^2 \\ \cdot \\ \cdot \\ \cdot \\ \lambda_1 P_1^n, \lambda_2 P_2^n, \cdots, \lambda_n P_n^n \end{bmatrix} \times \begin{bmatrix} (\underline{P}_1 \cdot H)h_1, (P_1 \cdot H)h_2, \cdots, (P_1 \cdot H)h_n \\ (P_2 \cdot H)h_1, \cdots, \\ \cdot \\ \cdot \\ \cdot \\ (\underline{P}_n \cdot H)h_1, (P_n \cdot H)h_2, \cdots, (P_n \cdot H)h_n \end{bmatrix} \tag{15}$$

which gives the following complicated expression for the general (i,j) entry of KH:

$$(KH)_{ij} = \frac{h_j \sum_{k=1}^{n} (\lambda_k P_k^i)(\underline{P}_k \cdot H)}{\sum_{k=1}^{n} \lambda_k (\underline{P}_k \cdot H)^2} \tag{16}$$

For the special case of i = j = 1, we can evaluate (16) for the one and two component measurement as follows:

a. One Variable Case: $H = (h_1, 0, 0, \cdots, 0)$

$$(KH)_{1,1} = \frac{h_1^2 \sum_{k=1}^{n} \lambda_k (P_k^1)^2}{h_1^2 \sum_{k=1}^{n} \lambda_k (P_k^1)^2} = 1 \tag{17}$$

or a perfect update as expected. [Note that $\underline{P}_k \cdot H = P_k^1 h_1$]

b. Two Variable Case: $H = (h_1, h_2, 0, 0, \cdots, 0)$

In this case, the $(KH)_{11}$ and $(KH)_{22}$ entries become:

$$(KH)_{11} = \frac{h_1\{\lambda_1 P_1^1 (P_1^1 h_1 + P_1^2 h_2) + \lambda_2 P_2^1 (P_2^1 h_1 + P_2^2 h_2)\}}{\lambda_1 (\underline{P}_1 \cdot H)^2 + \lambda_2 (\underline{P}_2 \cdot H)^2} \tag{18}$$

and

$$(KH)_{22} = \frac{h_2\{\lambda_1 P_1^2 (P_1^1 h_1 + P_1^2 h_2) + \lambda_2 P_2^2 (P_2^1 h_1 + P_2^2 h_2)\}}{\lambda_1 (\underline{P}_1 \cdot H)^2 + \lambda_2 (\underline{P}_2 \cdot H)^2} \tag{19}$$

Although the expressions are complicated, they do indicate that the more significant are the values of $(\underline{P}_1 \cdot H)$ and

$(\underline{P}_2 \cdot H)$ the more orthoganal are the measurement plane and P_f eigenvectors and the greater the resulting change or update in the covariance entry. It is noticed that if $\lambda_1(\underline{P}_1 \cdot H)^2$ in much greater than $\lambda_2(\underline{P}_2 \cdot H)^2$ then the following approximation can be made:

$$(KH)_{11} = \frac{h_1 P_1^1}{P_1^1 h_1 + P_1^2 h_2} \tag{20}$$

and

$$(KH)_{22} = \frac{h_2 P_1^2}{P_1^1 h_1 + P_1^2 h_2} \tag{21}$$

which varies the quality update between variables 1 and 2 according to the relative values of $P_1^1 h_1$ and $P_1^2 h_2$.

4. <u>The State-Error Update</u>

The actual error update vector is given as

$$\delta\hat{x} = KZ$$

or

$$\delta\hat{x} = \frac{(P_f H^T)}{\sum_{k=1}^{n} \lambda_k (\underline{P}_k \cdot H)^2} \tag{22}$$

which reduces to

$$\delta\hat{x} = [P][\lambda] \begin{bmatrix} \underline{P}_1 \cdot H \\ \underline{P}_2 \cdot H \\ \cdot \\ \cdot \\ \cdot \\ \underline{P}_n \cdot H \end{bmatrix} \frac{(z)}{\sum_{k=1}^{n} \lambda_k (\underline{P}_k \cdot H)^2} \tag{23}$$

or

$$\delta\hat{x} = \begin{bmatrix} \sum_{k=1}^{n} P_k^1 \lambda_k (\underline{P}_k \cdot H) \\ \sum_{k=1}^{n} P_k^2 \lambda_k (\underline{P}_k \cdot H) \\ \cdot \\ \cdot \\ \cdot \\ \sum_{k=1}^{n} P_k^n \lambda_k (\underline{P}_k \cdot H) \end{bmatrix} \frac{(*)}{\sum_{k=1}^{n} \lambda_k (\underline{P}_k \cdot H)^2} \tag{24}$$

which is a new and useful way of looking at the gain vector, K. If $\underline{P}_k \cdot H \approx 1$ for some subset of k, then the update of δx_1 will be proportional to the λ_k of the subset and the degree of nonorthoganality between $\underline{P}_k$ and H. Let us assume for the sake of argument that the subset of k has only one significant k called $\bar{k}$ [high $\lambda_{\bar{k}}(\underline{P}_{\bar{k}} \cdot H)$]; the update for $\delta\hat{x}_1$ can then be expressed as

$$\delta\hat{x}_i = \frac{P_{\bar{k}}^i Z}{(\underline{P}_{\bar{k}} \cdot H)} \tag{25}$$

which tends to favor those state variables, x_i, with a high $P_{\bar{k}}^i$ value. This measure will be explored along with others in the next section.

E. Performance Measures

1. General Remarks

The present section develops some potentially useful performance measures for the Kalman filter update based on a diagonalization or principal component analysis of the covariance matrix. According to Hotelling[4], Morrison[5], et al.; the eigenvalues of the covariance represent the entropy or uncertainty of the filter model with respect to the particular

eigenvector associated with that eigenvalue. With respect to a given eigenvector, $\underline{P}_i$, it is desirable to have the measurement plane as nearly perpendicular to $\underline{P}_i$ in n-space as is possible; for example, if the filter had a large uncertainty in the x-direction, a measurement perpendicular to the x-axis would completely remove the uncertainty in x. In general, it follows that a measurement where $\cos(\lambda_i) = \frac{(\underline{P}_i \cdot H)}{|H||\underline{P}_i|}$ is near unity represents a measurement where an uncertainty level equal to the eigenvalue, λ_i, can be removed from the filter according to a measurement defined by the component values of the normalized eigenvector, $\underline{P}_i$.

2. Geometric Interpretation of the Kalman Update

The variation of the eigenvalue/eigenvector structure of P_f^- will now be described for thte three measurement case (Table B4 of Appendix B) consisting of a compass measurement, an Autofocus measurement, and a doppler vertical velocity measurement. Because of the linearized, extended Kalman filter assumption, the order of the measurement sequence is irrelevant. The update time, for no particular reason, is chosen at 3.2 minutes into the trajectory. Only five eigenvalues of P_f^- before update are significant; they are listed in order of magnitude as 7.7×10^4, 8.8×10^3, 2.6×10^3, 2.6×10^3, and 1.1×10^3 respectively. According to its eigenvector, the largest eigenvalue, 7.7×10^4, represents uncertainty primarily in the altitude variable, the vertical velocity, and in the strongly correlated barameter altimeter bias variable. Since this eigenvalue does not express filter uncertainty concerning the velocity vector, it would be expected that the cos (α_1) value associated with the Compass velocity update would be small as in fact it is with a

value of only 2.29×10^{-5}. Only two eigenvalues, $\lambda_3 = 2.56 \times 10^3$ and $\lambda_4 = 2.55 \times 10^3$, have significant eigenvector components corresponding to the components of the velocity vector. The $\cos(\alpha)$ associated with these λ are 0.976 and 0.216 respectively which suggests, from the above discussion, that the optimum least squares Kalman update will primarily reduce the eigenvalue uncertainty associated with the $\cos(\alpha) = 0.976$ update; this, in fact, occurs with the updated P_f, after compass update, possessing only four rather than five significant eigenvalues with the λ_3 eigenvalue no longer appearing. In qualitative terms the update has absorbed into the filter that information corresponding to the $(\lambda_4 \underline{P}_4)$ eigenvalue/eigenvector pair. The other eigenvalue/eigenvector pairs are not significantly effected by the Compass update since their respective $\underline{P}_i$ vectors are nearly collinear with the compass measurement plane.

The second measurement, Autofocus, has its measurement plane orthogonal to the eigenvector, $\underline{P}_2$, with an eigenvalue weighting of $\lambda_2 = 2.56 \times 10^3$. After the Autofocus update, the λ_2 eigenvalue has been reduced to zero and is no longer significant. Since the sum of the eigenvalues equals the trace of the covariance matrix or the uncertainty level of the filter, it follows that each measurement will remove a level of uncertainty proportional to the eigenvalue corresponding to a high $H \cdot \underline{P}_i$.

The doppler vertical velocity measurement is the third and final measurement. The doppler measurement row vector $(0,0,0,0,0,1,0,\cdots,0)$ was found to have significant $H \cdot \underline{P}_i$ values

of (0.12,0.18,0.96) with respect to the first three eigenvectors of the updated P_f matrix. The V_Z or doppler measurement is especially significant for velocity vector update since one of the high $H \cdot \underline{P}_i$ eigenvectors is associated with the largest (7.6×10^4) eigenvalue and has significant $\lambda_1 P_{1j}$ values for the $j = 4,5,6$ components of the velocity vecotr. Accordingly, it would be expected that the addition of the doppler update would significantly improve the velocity update. This update enhancement has been observed repeatedly during the simulation runs.

3. Performance Measure for the Velocity Vecotr Update

It is worthwhile at this point to remind the reader of the overall project objective. Referring to Appendix A, the original project intent was to consider the use of the Autofocus measurement as a way of updating an INS navigation system in order to accurately estimate the velocity vector as a means of extending the "lock-in" time for the Autofocus algorithm. (See Appendix A)

Considering the diagonalization of P_f, it is clear from the above discussion that the degree of filter uncertainty about a given state variable i can be expressed as R_i where

$$R_i = \sum_{k=1}^{n} \lambda_k P_k^i \tag{26}$$

and n equals the order of the filter while P_k^i is the ith component of the normalized k^{th} eigenvector (see Morrison [6]). It would seem reasonable to expect that any useful measurement of the i^{th} variable would result in a decrease in R_i with the relative change in R_i expressing the relative effectiveness of the measurement. Furthermore, after a series of measurements, the dominant $\lambda_k P_k^i$

of the final R_i will indicate, by the significant components of P_k^{ℓ} ($\ell = 1,\cdots,N$), how an additional measurement should be designed in order to improve the filters knowledge of the i^{th} variable.

As an example of the monotonic decrease in R_i with each successive update, consider the R_i for the 6 observable variables over the three measurements; compass, Autofocus, and vertical velocity.

	Before Update	Compass Alone	Autofocus and Compass	Compass; Autofocus; and Doppler
Longitude	$6.71\text{x}10^{-4}$	$3.71\text{x}10^{-4}$	$1.70\text{x}10^{-4}$	$3.97\text{x}10^{-7}$
Latitude	$5.81\text{x}10^{-4}$	$4.44\text{x}10^{-4}$	$2.04\text{x}10^{-4}$	$1.34\text{x}10^{-6}$
Altitude	$7.68\text{x}10^{4}$	$7.5\text{x}10^{4}$	$7.39\text{x}10^{4}$	$4.34\text{x}10^{4}$
East Velocity	$1.95\text{x}10^{3}$	$1.00\text{x}10^{3}$	$4.93\text{x}10^{2}$	$4.34\text{x}10^{-7}$
North Velocity	$3.05\text{x}10^{3}$	$2.32\text{x}10^{3}$	$1.06\text{x}10^{3}$	$9.37\text{x}10^{-7}$
Vertical Velocity	$1.22\text{x}10^{4}$	$6.79\text{x}10^{3}$	$6.52\text{x}10^{3}$	$5.59\text{x}10^{-6}$

TABLE E1: Evaluation of R_i:t = 192 sec.

Strictly from an information content point of view, the great reduction in R_i for the longtiude, latitude, and velocity vector components indicates that the filter has confidence in its knowledge of these variables. Only the altitude variable retains a high R_i which suggests that this variable is really uncoupled from the other variables and can be updated without any interaction with the other variables. Furthermore, collapsing values of R_i indicate that any update error after the three measurements is the result

of either unmodeled truth state variables or measurement noise ; it is not the result of filter uncertainty.

Perhaps the greatest value of the R_i measure lies in the insight it provides for the design of the overall measurement strategy. Let us suppose that we wish to design a series of measurements that will accurately estimate the velocity vector. Before any measurement occurs at t = 3.2 minutes into the flight, the R_i for the three velocity components are given as follows: ($R_4 = 1.95\text{x}10^3$; $R = 3.05\text{x}10^3 \cdot R_6 = 1.22\text{x}10^4$). From inspection, it is determined that the λ_3, λ_4 eigenvalues contribute $\lambda_3 P_3^6 + \lambda_4 P_4^4 = 1.95\text{x}10^3$, $\lambda_3 P_3^5 + \lambda_4 P_4^5 = 3.05\text{x}10^3$, $\lambda_3 P_3^6 + \lambda_4 P_4^6 = 0.28$ to the values of R_4, R_5, R_6 respectively. In other words, the $(\underline{P}_3, \underline{P}_4)$ eigenvectors represent essentially the entire filter (V_E, V_N) uncertainty at this stage of the update. The first six observable components are given for $\underline{P}_3$ and $\underline{P}_4$ as follows:

$$\underline{P}_3 = (3.3\text{x}10^{-6}, 4.00\text{x}10^{-8}, -2.14\text{x}10^{-6}, \underline{0.977}, \underline{0.21}, \ 2.14\text{x}10^{-4}, \cdots)$$

and

$$\underline{P}_4 = (-7.4\text{x}10^{-8}, 1.8\text{x}10^{-6}, 9.6\text{x}10^{-6}, \ \underline{-0.215}, \underline{0.977}, \ -1.03\text{x}10^{-4}, \cdots)$$

It is clear that a measurement involving only the V_E, V_N velocity components would remove a significant amount of uncertainty concerning the V_E, V_N components; the Compass measurement is one such candidate measurement. After the Compass measurement, the $\underline{P}_2$ eigenvector of the new P_f matrix represents virtually all the R_i value for both the east and north velocity components at this point in the update process. The new $\underline{P}_2$ after Compass update is given as follows:

$$\underline{P}_2 = (1.45\text{x}10^{-7}, 1.73\text{x}10^{-7}, 9.86\text{x}10^{-6}, .421, .907, 1.47\text{x}10^{-4}, \cdots).$$

A simple calculation verifies that $\lambda_2 P_2^4$ and $\lambda_2 P_2^5$ represent nearly 100% of the R_4, R_5 values at this point in the update. The high values of P_2^4 and P_2^5 suggest that another (V_E, V_N) coupled measurement is indicated; namely, the Autofocus measurement. The principal uncertainty in the third velocity component, V_Z, however resides in the $\underline{P}_1$ eigenvector which is associated with the largest eigenvalue, λ_1; the $\underline{P}_1$ eigenvector is given as

$$\underline{P}_1 = (-5.29\text{x}10^{-12}, -2.06\text{x}10^{-11}, \underline{-0.981}, 4.33\text{x}10^{-6}, -9.3\text{x}10^{-6}, \underline{-.123}, \cdots) \quad (29)$$

which indicates that only an altitude or a direct V_Z measurement can remove the uncertainty in V_z.

After the Autofocus measurement has been completed, there are still significant values of R_4, R_5, R_6 which now reside almost entirely in the new $\underline{P}_1$ eigenvector given as

$$\underline{P}_1 = (3\text{x}10^{-8}, -3\text{x}10^{-9}, \underline{-0.98}, 9.1\text{x}10^{-3}, 1.9\text{x}10^{-2}, \underline{-0.121}, \cdots) \quad (30)$$

Because of the large values of the altitude and V_z components in the normalized $\underline{P}_1$, it would seem possible to remove the remaining uncertainty in the velocity vector by either a direct altitude or V_Z measurement. Taking the third measurement as a direct altitude measurement (Table(B12)), the R_5, R_5, R_6 values are reduced to (77.8, 168, 1030.) respectively which represent a decrease in the R_i values of (96.1%, 94.5%, 92.5%) which constitutes a good update. The simulation confirms this conclusion with the excellent velocity

vector mean error values of (20%, 16%, 33%). When the third scaler measurement is a direct V_Z measurement, the R_4, R_5, R_6 values are from Table (E1) reduced to zero. This indicates that, within the capabilities of the filter model, an optimum filter update will be realized by the Compass, Autofocus, and V_z measurements; this is verified in Table (B4) with mean error values of (17%, 11%, 2.22%) which represent the best velocity vector update observed. The zero values of R_4, R_5, R_6 further suggest that no additional velocity update improvement is possible when a fourth altitude measurement is added. This is confirmed in Table (B5) with an essentially unchanged mean value of (17%, 11%, 3.3%). As far as the velocity vector is concerned, the altitude measurement is superfluous.

The above discussion suggests the following step-by-step measurement strategy:

1. Determine the significant $\lambda_k P_k^i$ terms in the R_i values of interest.
2. Design (within practical limits) your measurement so that $H \cdot P_k \simeq 1.0$ for the important k values
3. Proceed until all R_i of interest are $\simeq 0$.

F. Addition of the Autofocus Line of Sight Term

Throughout the report, the assumption has been made that only a centripedal acceleration contributes to the quadrative phase error measured by the A.F. image restoration algorithm. Operationally, this would only apply to a circular loiter trajectory. For more generality, the line of sight acceleration component is added to the measurement as given by (See Appendix A):

$$\text{(Additional Term)} = K_{L.O.S.}\{\vec{A}_T \cdot \mu^T_{L.O.S.} - \hat{\vec{A}} \cdot \hat{\mu}_{L.O.S.}\} \tag{31}$$

where $\vec{A}_T$, $\hat{\vec{A}}$ are the true and best estimates of the acceleration vector and $\mu^T_{L.O.S.}$, $\hat{\mu}_{L.O.S.}$ are the true and best estimates of the line of sight unit vector connecting the aircraft to the target point. The proportionality constant $K_{L.O.S.}$ equals where λ is the wavelength of the radiation. The unit vector $\mu_{L.O.S.}$ can be expressed as

$$\vec{\mu}_{L.O.S.} \; (\cos[\alpha+\epsilon_E], \cos[\beta+\epsilon_N], \cos[\gamma+\epsilon_Z]) \tag{32}$$

where (α,β,γ) are the angles from the aircraft to the target and $(\epsilon_E, \epsilon_N, \epsilon_Z)$ are the altitude error vectors. Expression (32) now involves nine new state variables including an augmented delayed velocity vector used to form the acceleration vector.

In the SOFE simulation, the acceleration vector is formed as follows,

$$\hat{\vec{A}} \simeq \frac{\vec{V}_t - V_{t-T}}{T} \tag{33}$$

where $\vec{V}_{t-T}$ is the previous velocity stored in the H Z routine. In order to implement (33) and (32), the SOFE simulation was converted from variable step to a fix step integration with a value T = 0.5 seconds finally chosen.

Various runs were made with the L.O.S. component in the vicinity of t = 1000 seconds or 16 minutes into the flight. One outstanding change was the number of observable variables which increased from 6 in to centripedal only case to 12 in the L.O.S. case according

to the inner product test; however, the non-zero inner products were of the order of 0.2 instead of 0.7 for the previous case. While this suggests a "broader" coupling of the Autofocus measurement with the state vector, it also suggests a "weaker" coupling for the individual state variables. Some actual simulation runs are given in Tables (B13), (B14), and (B15); they are to be compared to the centripedal-only runs of Tables (B1), (B2), and (B4). While there are slight differences, it can be concluded that the addition of the L.O.S. term does not in general improve the velocity vector update. This is not too surprising since the addition of the L.O.S. term merely repositions the Autofocus measurement plane; it still remains a single, high S/N measurmeent although it does involve the state vector more intimately.

During the update, the L.O.S. runs exhibited the same geometric behavior among λ_i, $\underline{P}_i$ and H as the centripedal only runs although the uncertainty in the P_f matrix is now distributed over 8 eigenvectors rather than 5. As a consequence of this dispersion, each of the scaler measurements remove a lower percentage amount of uncertainty than in the centripedal only case. These conclusions are tentative however and must await the programming of the R_j calculation and the running of L.O.S. case over different intervals of the trajectory. Because of major programming problems, these tests could not be made within the contract time interval.

G. Topics to be Investigated

The project has suggested the following topics for investigation:

1. To put the inner product test (Equation (1)) on a firmer analytical foundation. To investigate the significance of "degree of observability" and how it can be used.
2. To complete the analysis and consideration of the L.O.S. Autofocus mode.
3. To further develop the geometric interpretation of the high S/N Kalman update. To put the performance measure, R_1, on a stronger analytical base and to also develop new performance measures for evaluating filter performance.
4. To investigate the value of the P_f diagonalization in the prediction and avoidance of filter divergence.
5. To consider systems where nonobservability can be a problem and to consider how the P_f diagonalization may help alleviate the problem.
6. To consider new applications and to demonstrate the value of the design philosophy defined in this report for arbitrary A and H matrices.

IV. CONCLUSIONS

The conclusions of the project are the following:

1. For the centripedal acceleration case only, the Autofocus measurement proved to be a useful measurement when supplemented by additional measurements. In particular, a Compass, an Autofocus, and doppler velocity update realize better than a 94% update quality. Without the Autofocus, the quality suffers greatly.

2. A geometric interpretation of the Kalman update was made. It was discovered that the relative orthoganality $(H, \underline{P}_i)$ of the eigenvectors of $\underline{P}_f$ to the rows of the measurement matrix, H, determine the update mechanisms. The Kalman update equations were analyzed and restated to reflect this interpretation.

3. A new performance measure, $\sum_{i=1}^{n} \lambda_i P_i^k = R_k$, was defined to reflect the relative uncertainty of the filter with regard to the k^{th} state variable. The measure, R_k, was used along with a study of $(\lambda_i, \underline{P}_i)$ combinations in order to define a measurement design philosophy.

4. The line of sight (L.O.S.) term was added to the Autofocus measurement and the resulting runs were discussed.

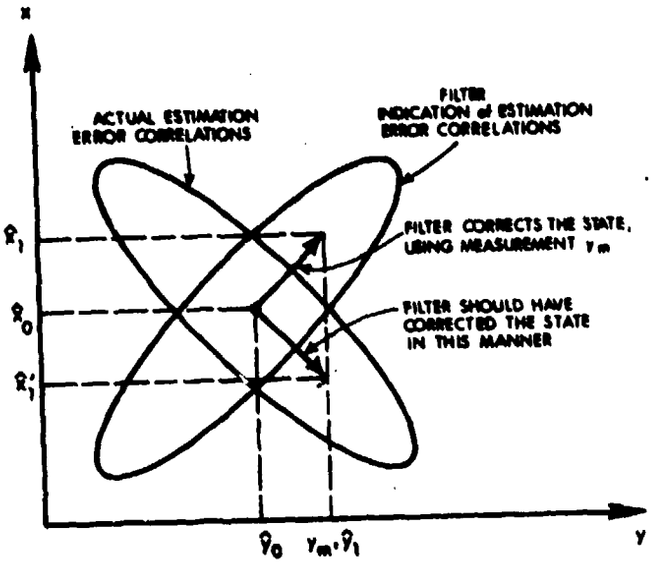

Figure 1: Geometric Interpretation of Kalman Filter Update

REFERENCES

1. S.H. Musick, "SOFE: A Generalized Digital Simulation for Optimal Filter Evaluation User's Manual," AFWAL-TR-80-1108.

2. T. Kailath, Linear Systems, (Prentice Hall, Englewood Cliffs, N.J., 1980), p. 135.

3. A. Gelb, Applied Optimal Estimation, (MIT Press, Cambridge, Mass., 1974), p. 237.

4. H. Hotelling, "Analysis of a Complex of Statistical Variables into Principal Components," Journal of Educational Psychology, vol. 24 (1933), pp. 417-441, 498-520.

5. D.F. Morrison, Multivariate Statistical Methods, (McGraw-Hill, New York, N.Y., 1967), pp. 221-258.

APPENDIX A

IMAGING RADAR AUTOFOCUS UPDATE OF AN INERTIAL NAVIGATION SYSTEM BY MEANS OF A KALMAN FILTER

by

William S. McCormick

ABSTRACT

The [illegible] an Autofocus update of an INS is investigated. Three cases are [illegible]d: (1) centripedal acceleration only; (2) centripedal and line-[illegible] acceleration; and (3) centripedal and line-of-sight acceleration as well as attitude error effects. The extended Kalman filter configuration was employed using the versatile SOFE Monte Carlo simulation program. Measurement matrices were defined for each of the three cases. Simulation results indicated an observability problem for Case (1). Suggestion for further work was included.

ACKNOWLEDGEMENT

The author would like to thank the Air Force Systems Command, the Air Force Office of Scientific Research and the Southeastern Center for Electrical Engineering Education for providing an interesting and productive summer at the Avionics Lab of Wright Patterson Air Force Base, Dayton, Ohio.

In particular, he would like to extend special thanks to Stanton Musick, Dr. Jack Bell, and Mrs. Sandra Benning for their continued help throughout the summer.

I. INTRODUCTION

Imaging radar (SAR) has become an increasingly important all weather sensing technique for both reconnaissance and weapon delivery applications. Briefly stated, imaging radar provides high azimuth resolution by coherently processing the naturally occurring doppler return over the synthetic radar aperture. Because of the phase coherence requirement, any phase error accumulated over the aperture time will result in both a loss of resolution and a higher sidelobe level. Under normal circumstances, the radar processor will use the dynamic output of the inertial navigation system (INS) to compensate for aperture phase perturbations. Unfortunately, a typical unaided INS system will have an error state vector that increases with time until the imaging performance of the SAR radar becomes seriously degraded.

In order to correct for the uncompensated phase error, a number of iterative image restoration techniques have been developed under the generic name of "Auto-Focus" (AF) techniques. Although the details of the algorithms are propietary, most autofocus techniques estimate various orders (e.g. quadratic, cubic, etc.) of phase error by measuring the relative displacement of a point target as processed in contiguous subarrays. Since the AF techniques must attempt a location estimate of a point target and since that target resolution is itself degraded by the phase error, it naturally follows that there will be a "lock-in" value for maximum accumulated phase error that must not be exceeded for successful autofocus operation. However, since the Auto-Focus algorithm is quite accurate and can essentially eliminate the phase error (provided it is operating within its "lock-in" range), it could also provide a potentially useful means of updating the INS system every aperture time. Assuming the AF scaler measurement contains adequate information on the INS error state vector, it would therefore appear possible to bound the growth of the error state vector by somehow integrating the AF measurement with the INS system. Performed optimally, such an AF update could well improve the INS-dependent SAR processor to such an extent that the AF mission time ("lock-in") is extended well beyond its present limit.

The optimal integration or augmentation of various sensors has traditionally been performed using the Kalman filter algorithm. Many

sensors[1] have been considered for INS augmentation including doppler radar, monopulse position fixing, star-trackers and loran/Omega type systems. No consideration has, however, been given to the potential value of AF algorithms as an INS update. With regard to the AF-INS Kalman filter update, a number of questions must be addressed. Some of these questions are as follows:

(1) questions of observability or simply whether the scaler AF measurement contains enough information about the INS error state-vector to provide a useful filter update.

(2) given the nonlinear nature of the AF measurement, the effects of trajectory dependent nonlinear noise must be considered.

(3) since the Kalman filter will have a delayed state vector, the question of filter convergence must be investigated when the AF update is used.

II. OBJECTIVES

The principal objective of this study was to investigate the value of an "Auto-Focus" update of an INS using the Kalman filter algorithm. In particular, as discussed in Section I, the study will consider the value of the AF update as a means of extending the AF mission time or, equivalently, the time before the AF algorithm loses lock. A detailed consideration of observability, the effects of nonlinear noise and filter convergence will be considered for the following cases:

Case A: In the simplest case, only the centripedal acceleration term is considered as a contributor to quadratic phase error. This case implicitly assumes that the velocity vector is constant which is clearly an oversimplification. Since this measurement comprises only one scaler measurement and involves only 3 of the 13 state-variables, the question of observability is very important in this case.

Case B: For this case, the line of sight acceleration component is included as a source of quadratic phase error. Such a measurement is still scaler and nonlinear but now involves 9 of the 13 state-variables.

Case C: The attitude error states are included in their measurement which increases the total number of state-variables involved in the measurement to 12.

Case D: Using the complete measurement of the 12 state-variable dependent AF update of Case C, an investigation will be made into the performance degradation suffered by the Kalman filter when its measurement matrix is defined by the more computationally efficient assumptions of Cases A and B.

III. EVALUATION OF QUADRATIC PHASE ERROR

As developed in reference 2, the RF phase, $\Psi(t)$, generated by aircraft motion over the aperture time can be represented in a Taylor series as,

$$\Psi(t) = \left(\frac{4\pi}{\lambda}\right) [R(o) + [\dot{R}(t)]_{t=o} t + [\ddot{R}(t)]_{t=o} \frac{t^2}{2} + \ldots + \tag{1}$$

It is assumed in this study that the phase return is predominately low-frequency in origin and can be approximated well by neglecting third and higher order terms from (1); that is, the phase variation, $\Psi(t)$, varies quadratically with time. With reference to the autofocus measurement, the phase error can be expressed directly as,

$$\Psi_\varepsilon(t) = \Psi_T - \Psi_E = \left(\frac{4\pi}{\lambda}\right) \left\{ [R_T - R_E]_{t=o} + [\dot{R}_T - \dot{R}_E]_{t=o} t + [\ddot{R}_T - \ddot{R}_E] \frac{t^2}{2} + \ldots + \right\} \tag{1a}$$

where the subscript T represents true value and the subscript E represents estimated value. After every aperture interval, T, the autofocus algorithm provides an estimate of the quadratic error term given by

$$\Psi_{\varepsilon \left\{ \begin{array}{l} \text{Auto focus} \\ \text{Quadratic} \\ \text{Evaluated} \\ \text{at } t=T \end{array} \right\}} = \left(\frac{4\pi}{\lambda}\right) [\ddot{R}_T - \ddot{R}_E] \frac{T^2}{2} \tag{1b}$$

Referring the differential diagram of Figure 1, we can write

$$dR = - dx \cos \theta \tag{1c}$$

or

$$\frac{dR}{dt} = \dot{R} = - V \cos \theta \tag{1d}$$

or, after differentiating a second time,

$$\ddot{R} = V (\sin \theta) \frac{d\theta}{dt} - (\cos \theta) \frac{dV}{dt} \tag{2}$$

which, since $\frac{d\theta}{dt} = \frac{V \sin \theta}{R}$, will equal

$$\ddot{R} = \underset{(CENT.)}{\frac{(V \sin \theta)^2}{R}} - \underset{(L.O.S.)}{\left(\frac{dV}{dt}\right)} (\cos \theta) \tag{3}$$

which can be recognized as the sum of a centripedal term and a line of sight term. The autofocus output can then be expressed in terms of (1b) and (3) as

$$\underset{\varepsilon \left\{\begin{matrix}\text{Quadratic} \\ \text{Evaluated} \\ \text{at } t=T\end{matrix}\right\}}{\underline{\text{Auto focus}}} = \left(\frac{4\pi}{\lambda}\right) \frac{\sin^2 \theta \, T^2}{R} \left\{V_T^2 - V_E^2\right\}$$

[CENTRIPEDAL]

$$- \left(\frac{4\pi}{\lambda}\right) \{\vec{A}_T \cdot \vec{\mu}^T_{LOS} - \vec{A}_E \cdot \vec{\mu}^E_{LOS}\}$$

[L.O.S.] (4)

where μ^T_{LOS}, μ^E_{LOS} are the true and estimated unit line of sight vector. The unit vector, μ_{LOS}, points from the aircraft to the target and has direction cosines defined in the geographical frame. The terms V_T^2, V_E^2, represent the magnitude squared of the true and estimated velocities respectively.

In the study, the assumption is also made that the antenna phase center is coincident with the body centroid of the aircraft. This assumption merely neglects the lever arm effects between phase center and body center and is quite reasonable physically; it also offers a considerable simplification since it essentially equates the aircraft (INS) and antenna reference systems.

IV. THE EXTENDED KALMAN FILTER

A voluminous literature exists on the Kalman filter. Basically, it is a minimum variance, recursive estimator that generates the optimum conditional mean estimate. In the usual continuous-discrete measurement form, the linear Kalman filter propagates the estimate, $\underline{\hat{X}}(t)$, and covariance, $P_f(t)$, according to the dynamic equations,

$$\dot{\underline{\hat{X}}}_f(t) = F(t)\ \hat{\underline{x}}_f(t) \tag{5}$$

and

$$\dot{P}_f(t) = F(t)\ P_f(t) + P_f(t)\ F^T(t) + Q_f(t) \tag{6}$$

where $F(t)$, $Q_f(t)$ are the filter dynamics and input noise levels respectively. At measurement time, the filter weights the new measurement according to its signal to noise properties and by the current state of knowledge of the state vector as expressed by the propagated covariance, $P_f(t)$. The measurement and update operations are defined by the gain matrix, $\underline{K}$, as follows:

$$\underline{K} = P_f^- H^T [H\ P_f^-\ H^T + R_f]^{-1} \tag{7}$$

$$\hat{\underline{X}}_f^+ = \hat{\underline{X}}_f^- + \underline{K}\ [\tilde{Z}_s - H\ \hat{\underline{X}}_f^-] \tag{8}$$

$$P_f^+ = P_f^- - \underline{K}\ H\ P_f^- \tag{9}$$

where H is the measurement sensitivity matrix, $\underline{R}_f$ is the measurement noise covariance, and $\hat{Z}_s$ is the measurement itself.

Since both the INS dynamics and the autofocus measurements are highly nonlinear, the above linear Kalman filter cannot be directly applied in the form of equation 5 through 9. Rather, the extended Kalman filter is used where the $F(t)$, $H(t)$ are now linearized about some estimated trajectory as,

$$F(t;\hat{\underline{X}}_f) = \left.\frac{\partial f(X_f;t)}{\partial \underline{X}_f}\right|_{X_f = \hat{\underline{X}}_f} \tag{10}$$

and

$$H(t_i;\hat{\underline{X}}_f) = \frac{\partial\, h_f(X_f;t_i)}{\partial\, \underline{X}_f}\,\Bigg|\, \underline{X}_f = \hat{\underline{X}}_f \qquad (11)$$

Figure 2 illustrates the extended Kalman filter configuration.

Although Figure 2 represents the usual or direct configuration, it is not an attractive configuration for INS applications because of the high computational requirements involved in propagating the full vector estimate, $\hat{\underline{X}}_f(t)$. The indirect or error-state vector configuration is the approach normally used. This approach propagates the nonlinear, dynamic equation, $f(\underline{X}_f;t)$, by linearizing about the trajectory as is already done with the covariance propagation. The time variation of the error state-vector is much slower than the full state vector which therefore permits real time operation.

V. THE KALMAN FILTER SIMULATION USING "SOFE" WITH THE LN-15 INS DYNAMICS

In order to study the effectiveness and sensitivity of the nonlinear Kalman filter, a Monte Carlo simulation is usually performed. In such a simulation, the actual measurement is generated by what is referred to as the "truth" model which is simply a higher order model of the particular INS under investigation. For the sake of the simulation, the "truth" error state-vector, $\underline{X}_s(t)$, is considered as the actual error-vector which then allows the best Kalman estimate to be written directly as "true" + $\underline{X}_s(t)$ - $\underline{X}_f(t)$ where the "true" trajectory is a tape input corresponding to some maneuver. The measurement is now written as

$$\text{Measurement} = (\text{TRUE} - \text{PREDICTED}) + \text{NOISE} \qquad (12)$$

where the TRUE corresponds to the nonlinear measurement as given by the trajectory values and the PREDICTED is the nonlinear measurement as given by the best Kalman filter estimate, "True" + $\underline{X}_s(t)$ - $\underline{X}_f(t)$. The noise is white, Gaussian measurement noise with a covariance of R_f.

During the study, the versatile Monte Carlo simulation program called SOFE was used exclusively. This program was written by Mr. Stanton Musick of the WPAFB Avionics Lab and features a variable -5- step integration subroutine and the Carlson sequential square root matrix inversion routine for Kalman filter gain, $\underline{K}$, calculation.

The INS model chosen was the local-level Honeywell LN-15 system defined as a 1 n.m./hr.system. As listed in Appendix I, the "truth" model has 47 state variables and the filter model has 15 state variables.

VI. OBSERVABILITY TEST

Since the update on measurement constitutes an attempt to update a 13 state vector with a single scaler measurement, the question of observability becomes important. In the problem at hand, the question can be phrased as follows: "Is the implicit coupling of velocity, acceleration, and attitude components as contained in the LN-15 dynamics equations sufficient to allow the Kalman filter to update each vector component in the proper proportion."

As developed in reference 5, a measurement can be shown to be observable if the following observability matrix, Φ, is invertible;

$$\Phi = \left[H^T \;\vdots\; F^T H^T \;\vdots\; (F^T)^2 H^T \;\vdots\; \ldots \;\vdots\; (F^T)^{n-1} H^T \right] \tag{13}$$

the matrix is a square nxn matrix. The degree of observability of the measurement can be quantified by the condition number, C, of Φ defined as

$$C = \frac{\text{Determinant of } \Phi}{||\Phi||} \tag{14}$$

VII. THE MEASUREMENT AND H MATRICES FOR CASES A,B, AND C

Case A: Centripedal Acceleration Only

Referring to Section III, the measurement can be written directly as

$$K_{CENT} \left\{ (V_{T_e}^2 + V_{T_n}^2 + V_{T_z}^2) - (\hat{V}_e^2 + \hat{V}_n^2 + \hat{V}_z^2) \right\} = h_{\underline{s}}(\vec{V}_I, t) - h_{\underline{f}}(\vec{V}_E, t) \tag{15}$$

where $(V_{T_e}, V_{T_n}, V_{T_z})$ is the time velocity vector of the tape trajectory and (V_e, V_n, V_z) is the best estimate of velocity given by

$$\begin{aligned} \hat{V}_e &= V_{T_e} + XS(4) - XF(4) \\ \hat{V}_n &= V_{T_n} + XS(5) - XF(5) \\ \hat{V}_z &= V_{T_z} + XS(6) - XF(6) \end{aligned} \tag{16}$$

with $K_{CENT} = \dfrac{4\pi \sin^2 \theta \, T^2}{\lambda R}$.

where the first order perturbation of (13) yields the H matrix given as

$$H(4) = \frac{\partial h_f(\ )}{\partial \hat{V}_e}\bigg|_{\hat{V}_e} = -2K_{CENT}\,\hat{V}_e = -2K_{CENT}\,(V_{T_e} + XS(4) - XF(4))$$

$$H(5) = \frac{\partial h_f(\ )}{\partial \hat{V}_n}\bigg|_{\hat{V}_n} = -2K_{CENT}\,\hat{V}_n = -2K_{CENT}\,(V_{T_n} + XS(5) - XF(5)) \qquad (17)$$

$$H(6) = \frac{\partial h_f(\ )}{\partial \hat{V}_z}\bigg|_{\hat{V}_z} = -2K_{CENT}\,\hat{V}_z = -2K_{CENT}\,(V_{T_z} + XS(6) - XF(6))$$

In this case, the nonlinear noise is only second order and has an explicit expression, R_A, given as

$$R_A = K_{CENT}\left\{(XS(4) - XF(4))^2 + (XS(5) - XF(5))^2 + (XS(6) - XF(6))^2\right\} \qquad (18)$$

Case B: With Line of Sight But Without the Attitude Error

Referring again to Section III, the measurement term includes Case A plus the nonlinear term due to the line of sight acceleration given in (4) as

$$K_{L.O.S.}\,\{\vec{A}_T \cdot \vec{\mu}^T_{L.O.S.} - \hat{\vec{A}} \cdot \hat{\vec{\mu}}_{L.O.S.}\} \qquad (19a)$$

where $K_{L.O.S.} = \Psi\pi/\lambda$.

This can be expanded as

$$K_{L.O.S.}\,\{A_{T_e}\cos\alpha_T + A_{T_n}\cos\beta_T + A_{T_z}\cos\gamma_T$$

$$- \hat{A}_e\cos\hat{\alpha} - \hat{A}_n\cos\hat{\beta} - \hat{A}_z\cos\hat{\gamma}\} = h_s(\ ) - h_f(\ ) \qquad (19b)$$

where $(\cos\alpha_T, \cos\beta_T, \cos\gamma_T)$ and $(\cos\hat{\alpha}, \cos\hat{\beta}, \cos\hat{\ })$ are the true and estimated direction cosines of the unit vector between the target and the phase center and $\vec{A}_T$, $\hat{\vec{A}}$ are the true and estimated values of acceleration. All the quantities of expression (19b) are referenced to the geographical system.

Since the LN-15 INS dynamic equations are basically second order (Newton's second law), the acceleration state vector is implicit and can be generated dynamically as follows

$$\vec{A} = (\vec{V}_t - \vec{V}_{(t-\tau)})/\tau \qquad (20)$$

where $\vec{V}(t-\tau)$ is the velocity vector at the end of the previous integration

interval and τ is the size of the integration interval. The acceleration vector is augmented as XF(14), XF(15), X(16) respectively. The true and estimated values of the direction cosines are calculated in the geographic system from the true and estimated coordinates of the aircraft position relative to the fixed point target being imaged. The equations are straightforward and are not included here.

The derivation of the new entries of the H matrix proceeds from the general expression for $H\{t_i, \hat{x}_f\}$ given in (11) as

$$H(t; \underline{\hat{x}}_f) = \left.\frac{\partial h_f(\underline{x}_f; t_i)}{\partial x_{\underline{f}}}\right|_{x_{\underline{f}} = \hat{x}_{\underline{f}}} \tag{21}$$

where the new $h_f(\ )$ function is given by

$$h_f(x_{\underline{f}}; t) = K_{L.O.S.} \{\hat{A}_e \cos(\hat{\alpha}) + \hat{A}_n \cos(\hat{\beta}) + \hat{A}_z \cos(\hat{\gamma})\} \tag{22}$$

which leads directly to the following [H] matrix entries given as:

$$\begin{aligned}
H(1) &= K_{L.O.S.}\{-\hat{A}_e \sin(\hat{\alpha})\} \\
H(2) &= K_{L.O.S.}\{-\hat{A}_n \sin(\hat{\beta})\} \\
H(3) &= K_{L.O.S.}\{-\hat{A}_z \sin(\hat{\gamma})\} \\
H(14) &= K_{L.O.S.}(\cos(\hat{\alpha})) \\
H(15) &= K_{L.O.S.}(\cos(\hat{\beta})) \\
H(16) &= K_{L.O.S.}(\cos(\hat{\gamma}))
\end{aligned} \tag{23}$$

where

$$\begin{aligned}
\hat{A}_e &= A_{T_e} + XS(45) - XF(14) \\
\hat{A}_n &= A_{T_n} + XS(46) - XF(15) \\
\hat{A}_z &= A_{T_z} + XS(47) - XF(16) \ .
\end{aligned} \tag{24}$$

In calculating the expressions of (19b) and (23) the geographical frame is employed which requires a position conversion from the earth frame (λ,L) to

(X_e, X_n) in the geographical frame; e.g. $(\delta\hat{\alpha})$ geographical can be set equal to R/R_f $(\delta\hat{\lambda})$ $[R_f\ \delta\hat{\alpha} = R\ \delta\hat{\lambda}]$, with R equal to the earth-ellipsoidal radius length and R_f equal to the radius vector length from the image point target to the antenna phase center.

With regard to expression (19), the inclusion of position error in the form of $(\delta\hat{\alpha}, \delta\hat{\beta}, \delta\hat{\gamma})$ is a direct result of the imaging radar application where the unit pointing vector has one end fixed at the imaged point throughout the entire aperture time while the other vector end fluctuates according to the uncertainty of the aircraft position. Such a position uncertainty term is not present in the H-matrix of the doppler-INS augmentation since the doppler measurement is not referenced to specific target points; i.e. the unit vector merely slides along the ground in a parallel fashion and is not fixed at one specific target.

For Case B, the nonlinear noise term is the sum of the nonlinear noise of Case A and a remainder term of the Taylor series expansion of expansion of (19) which can be handled as follows

$$
\begin{aligned}
R_{(\text{remainder})} \leq \frac{1}{2} K_{\text{L.O.S.}} \Big\{ & |\hat{A}_e|_M |\delta\hat{\alpha}|_M^2 + |\hat{A}_n|_M |\hat{\delta\beta}|_M^2 \\
& + |\hat{A}_z|_M |\hat{\delta\gamma}|_M^2 + |\delta\hat{A}_e|_M^2 + |\delta\hat{A}_n|_M^2 \\
& + |\hat{\delta A}_z|_M^2 + |\hat{A}_e|\ |\delta\hat{\alpha}|_M |\delta\hat{A}_e|_M \\
& + |\hat{A}_n|\ |\hat{\delta\beta}|_M |\delta A_n|_M + |\hat{A}_z|\ |\delta\hat{\gamma}|_M |\delta\hat{A}_z|_M \Big\}
\end{aligned}
\tag{25}
$$

where the subscript, M, refers to the maximum value expected over normal operation. Since this term is not known apriori, it is impossible to compensate for; however, under normal convergence, the nonlinear noise is expected to be masked by measurement noise.

Case C: Attitude Errors Included

The attitude error vector in geographical coordinates is given as $\vec{\varepsilon} = (\varepsilon_e, \varepsilon_n, \varepsilon_z)$. Since the (α,β,γ) angles of (19b) are also defined with respect to the geographical system, we can simply add angles and extend expression (19b) for Case B to include Case C as follows:

$$K_{L.O.S.} \{\vec{A}_T \cdot \overrightarrow{\mu^T_{L.O.S.}} - \vec{\hat{A}} \cdot \overrightarrow{\hat{\mu}_{L.O.S.}}\} \tag{26}$$

or, with $\vec{\hat{\varepsilon}}$ included,

$$\begin{aligned} & K_{L.O.S.} \{A_{T_e} \cos \alpha_T + A_{T_n} \cos \beta_T + A_{T_z} \cos \gamma_T \\ & - \hat{A}_e \cos (\hat{\alpha} + \hat{\varepsilon}_e) - \hat{A}_n \cos (\hat{\beta} + \hat{\varepsilon}_n) \\ & - \hat{A}_z \cos (\hat{\gamma} + \hat{\varepsilon}_z)\} \\ & = h_s(\ ) - h_f(\ ). \end{aligned} \tag{27}$$

The new [H] entries corresponding to $\hat{\varepsilon}$ can be again calculated from the partial derivative expression of (11) directly as

$$\begin{aligned} H(7) &= K_{L.O.S.} \{\hat{A}_e \sin (\hat{\alpha} + \hat{\varepsilon}_e)\} \\ H(8) &= K_{L.O.S.} \{\hat{A}_n \sin (\hat{\beta} + \hat{\varepsilon}_n)\} \\ H(9) &= K_{L.O.S.} \{\hat{A}_z \sin (\hat{\gamma} + \hat{\varepsilon}_z)\}. \end{aligned} \tag{28}$$

VIII. COMPUTER RESULTS

A. General Remarks

Major problems were encountered during the simulation with filter divergence and the "debugging" of computer execution errors. With regard to the "debugging" problem, it is indeed unfortunate that the WPAFB Cyber CDC possesses such a poor execution error diagnostic; many hours were spent in intriguing but unnecessary searches for yet another mode error. On the other hand, the problem of filter divergence was not unexpected and could in general be traced to one or all of the following three contributors:

1. The effect of higher order terms resulting from the nonlinear nature of the Autofocus measurement.
2. The lack of observability (or whether there is enough information in the update) in the measurement itself, which will allow $|XS-XF|$ to accumulate indefinitely.
3. The reduced state nature of the filter model.

The SOFE simulations were generally run over an 80 sec. trajectory with a 4 or 8 sec. Auto-Focus update interval. The available trajectory was a low-speed, low-altitude trajectory with some degree of maneuvering present.

B. Case A:

Using the complete nonlinear measurement of (15), the early runs were found to be divergent; that is, the difference; $|XS-XF|$ became increasingly large. Originally, it was thought that the nonlinear noise contribution to the update [which, from simple algebra, can be expressed as $\{(DS')^2/2(V_T\ DS')\}$ where $DS'=XS-XF$ and V_T is the true velocity] was the fundamental cause of the divergence. To counteract this effect, the measurement noise was increased but still the filter remained divergent. To resolve the role of the nonlinear noise effect, the nonlinear or higher-order terms were simply subtracted thereby linearizing the measurement. This was possible only in Case (A) where the higher order term (2nd order) was known in closed form; it is, of course, impossible to subtract this term in practice since XS is unknown. However, the filter continued to remain divergent even with this extreme fix which seem to suggest that the higher order terms were not the fundamental cause of the divergence.

The next factor considered was model divergence or the effect of the reduced order of the filter error state-vector. The deleted state problem

is especially serious in the high measurement accuracy case (e.g. Autofocus) since the filter, as expressed by its propagated covariance, becomes over-confident as to the accuracy of its estimate and ignores further measurement updates. In such a situation, the subtle differences between the truth and filter are accentuated and the filter eventually diverges. The standard technique for controlling this type of divergence is to artifically inject noise into the propagating covariance either by increasing the initial covariances or by introducing ficticious process noise (Q_f terms). Both methods were tried and eventually a Q_f level of 320 ft/sec^2 in the velocity states was found effective in controlling divergence. Even though this intellectually unsatisfying approach did control gross divergence, the updates themselves were not anymore effective; that is, the Kalman gain vectors were not receiving and processing the reassurement in an effective manner. By a process of elimination, the question of observability therefore became the center of attention. Initially, the observability matrix of (13) was programmed on the computer with a term added, $\frac{d\{(F^T)^{i-1} H^T\}}{dt}$, to the $(F^T)^i H^T$ column to account for the time varying nature of F(t) as the operating point moved along the trajectory. Immediately, it became apparent that the 13 state observability matrix would be singular (zero determinant) because of the non-interactive longitude channel (first row of F) and the three (0) columns of the gyro-drift states. Accordingly, the 13 state matrix was reduced to 9 states and the program was rerun over the usual trajectory. The results indicated very marginal observability with the condition number of the Φ matrix lying between 0 and 10^{-20}! These results, of course, apply to this particular trajectory only; other trajectories may possess better observability particularly violent maneuvers where all three velocity components are non-zero and rapidly changing. As an added support for the observability argument, Appendix II presents a 2nd order system with a similar nonlinear measurement; the observability criterion indicates regions of non-observability in the (X_1, X_2) state space.

Although the properties of the observability matrix are an analytically satisfying way of investigating observability, a more direct way is to simply look at the change in covariance at update. Referring to Figure 3(a,b,c),

for a high ficticious Q_f in the velocity states of 32, only the north velocity component receives a significant update while the other velocity components and the 10 other state variables are essentially unaffected. Figure 4(a,b,c) shows the update effect for a lower Q_f of 3.2; in this case, the effect is less dramatic due to the lower absolute value of the covariance. However, the large correction at the first update is interesting and was also reflected in an excellent initial filter update. For some reason, the quality of the update was not maintained. Figure 5(a,b,c) gives the covariance propagation for $Q_F = 0$ when the filter becomes divergent. The rapid monotonic decrease in $\sqrt{P}_f$ is an indication of the filter's absolute confidence in its erroneous state estimate which leads finally to the divergence. From the covariance plots, it would therefore appear that only the north component of velocity is observable for this particular trajectory given the LN-15 dynamics. The system observability should however improve in Case (B) and Case (C) since more state variables are included in the measurement matrix.

C. Case B:

While conceptually straightforward, the inclusion of the acceleration state vector in the SOFE simulation proved to be quite difficult. A fixed step integration mode was used for simplicity but problems were encountered trying to circumvent the 5 step numerical integration routine that is a permanent feature of SOFE. Many mode or execution errors were encountered. It was only on the last day of the ten week period that a "successful" run was completed. Early results indicate an improvement in observability based on the propagated covariance. The conditioning of the observability matrix was not checked however.

A follow-on grant proposal will propose completing Cases B,C, and D and resolving the observability question.

IX. RECOMMENDATIONS

In a follow on grant proposal, I will recommend the following tasks:

(1) Cases B,C and D should be completed as outlined. Special attention should be given to the relative importance of observability and nonlinear noise in all three cases. It should be emphasized that only an investigation of the complete case (Case C) can resolve the potential value of the Autofocus update.

(2) If observability should continue to be a problem in Case C, the use of similarity transformations to isolate the observable and nonobservable states should be considered. The identification of the observable states could suggest additional state deletion or addition and also the type of additional sensor input necessary to augment the Autofocus update.

(3) Because the Autofocus measurement is essentially a high signal to noise ratio measure, the presence of nonlinear noise could seriously degrade its potential usefulness. Accordingly, the use of the iterated, extended Kalman filter should be considered.

(4) The use of the finite memory technique for controlling filter divergence should be investigated. This technique is intellectually more satisfying than merely adding a higher noise level to the covariance propagation.

(5) If and when a satisfactory update is realized, the effects of different trajectories and update intervals should be investigated.

(6) An adaptive Kalman filter configuration should also be considered. This suggestion is motivated by an observed improvement in attitude error observability when the appropriate H matrix entry was zeroed for velocity components below a certain threshold level.

REFERENCES

1. North Atlantic Treaty Organization, "Theory and Applications of Kalman Filtering," Published February, 1970.

2. R. Kitzerow, "Motion Compensation of Synthetic Aperture Radars (SAR)," Memorandum to AFSC/DLCAA, October, 1978.

3. S.H. Musick, "SOFE: A Generalized Digital Simulation For Optimal Filter Evaluation User's Manual," AFWAL-TR-80-1108.

4. W.S. Widnall and P.A. Grundy, "Inertia Navigation System Error Models," Intermetrics, TR-03-73, May 11, 1973.

5. A. Gelb, Applied Optimal Estimation, (MIT Press, Cambridge, Mass., 1974), p. 69.

6. S.H. Musick, "Radar Measurements and Measurement Matrices for EAR," AFAL-TM-76-48, May 12, 1976.

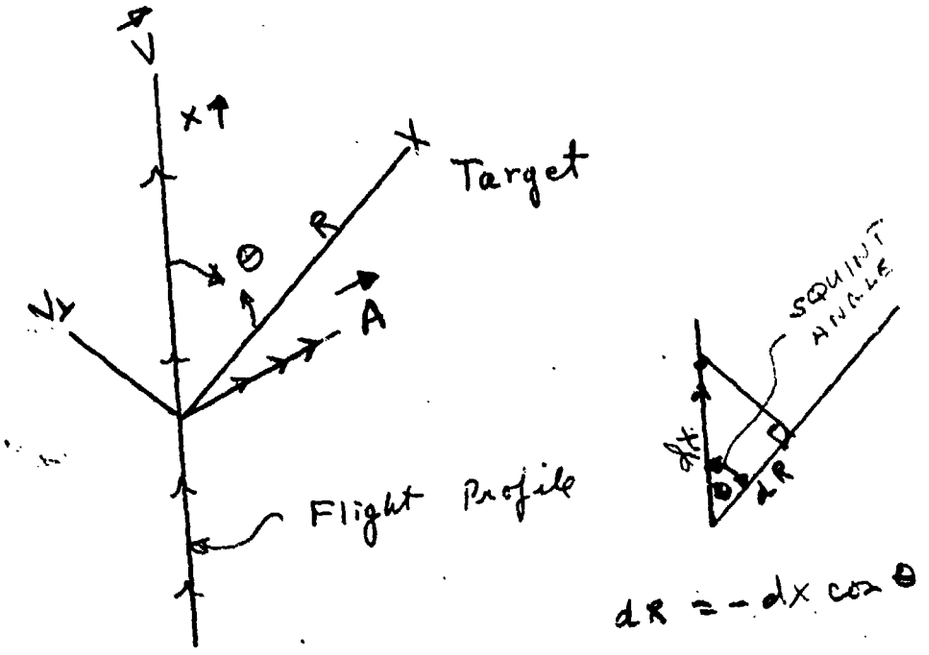

Figure 1: SAR Geometry

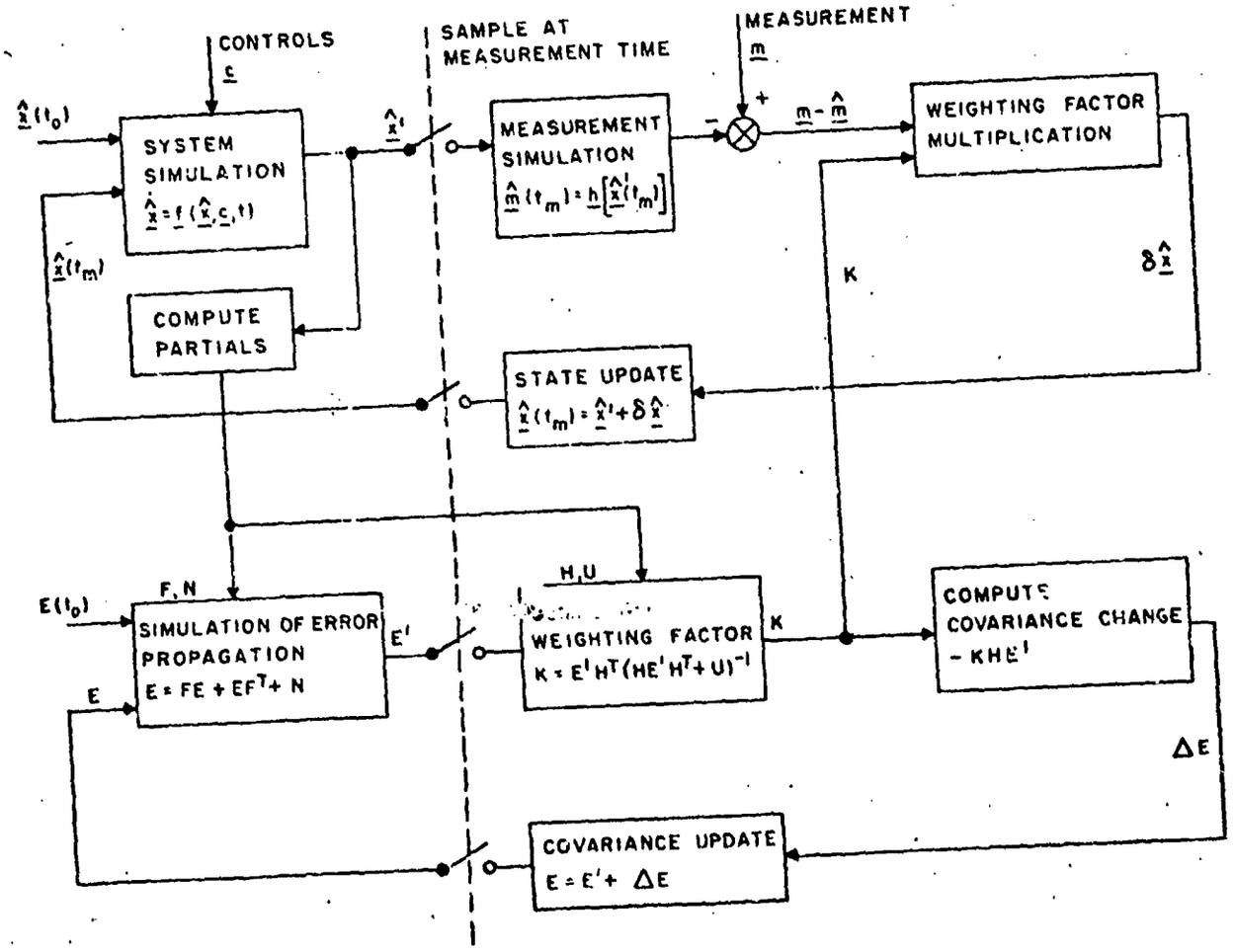

Figure 2: Extended Kalman Filter: Direct Configuration

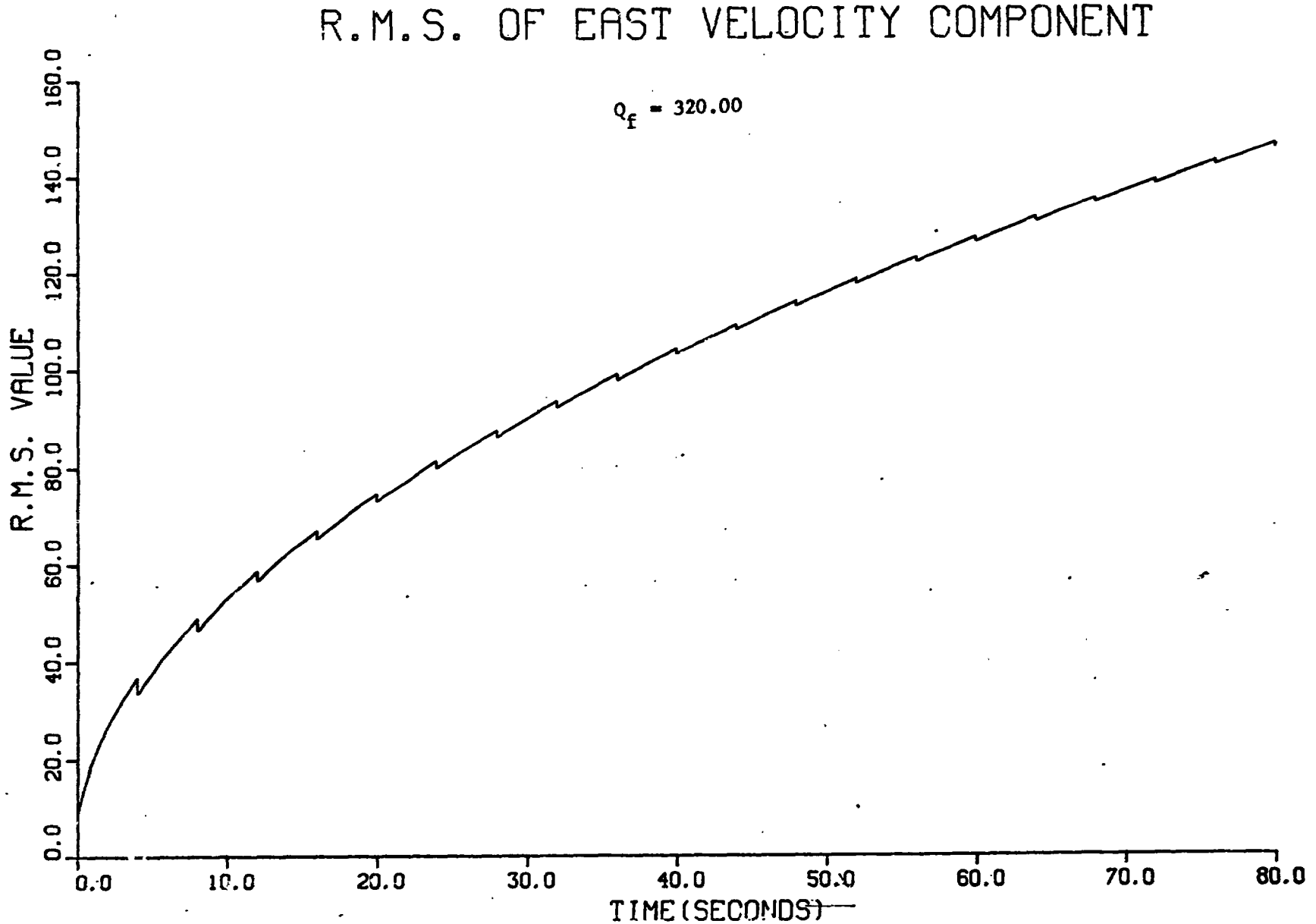

Figure 3-(a): R.M.S. OF EAST VELOCITY COMPONENT FOR Q_f = 320.0

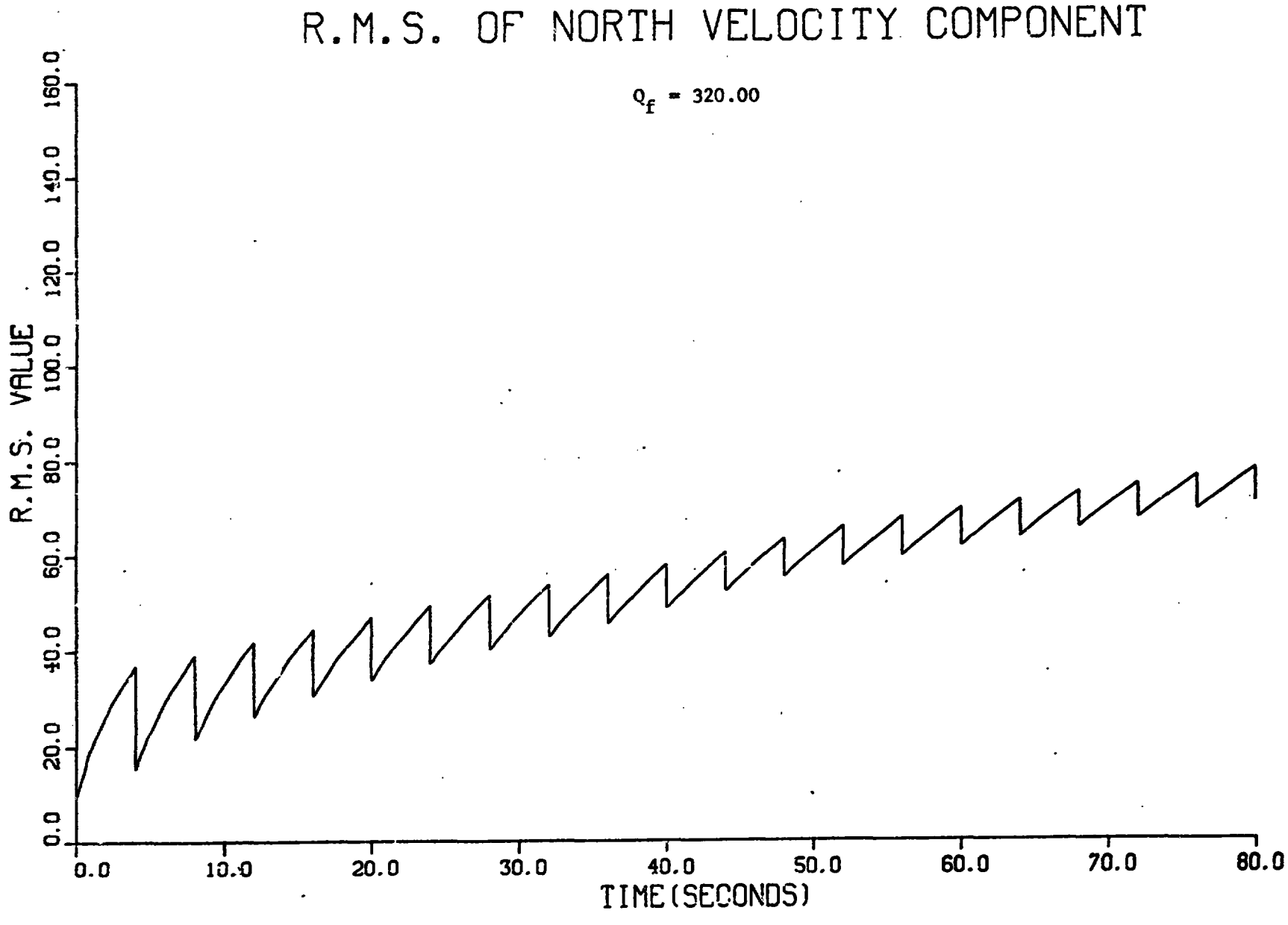

Figure 3-(b): R.M.S. OF NORTH VELOCITY COMPONENT FOR Q_f = 320.0

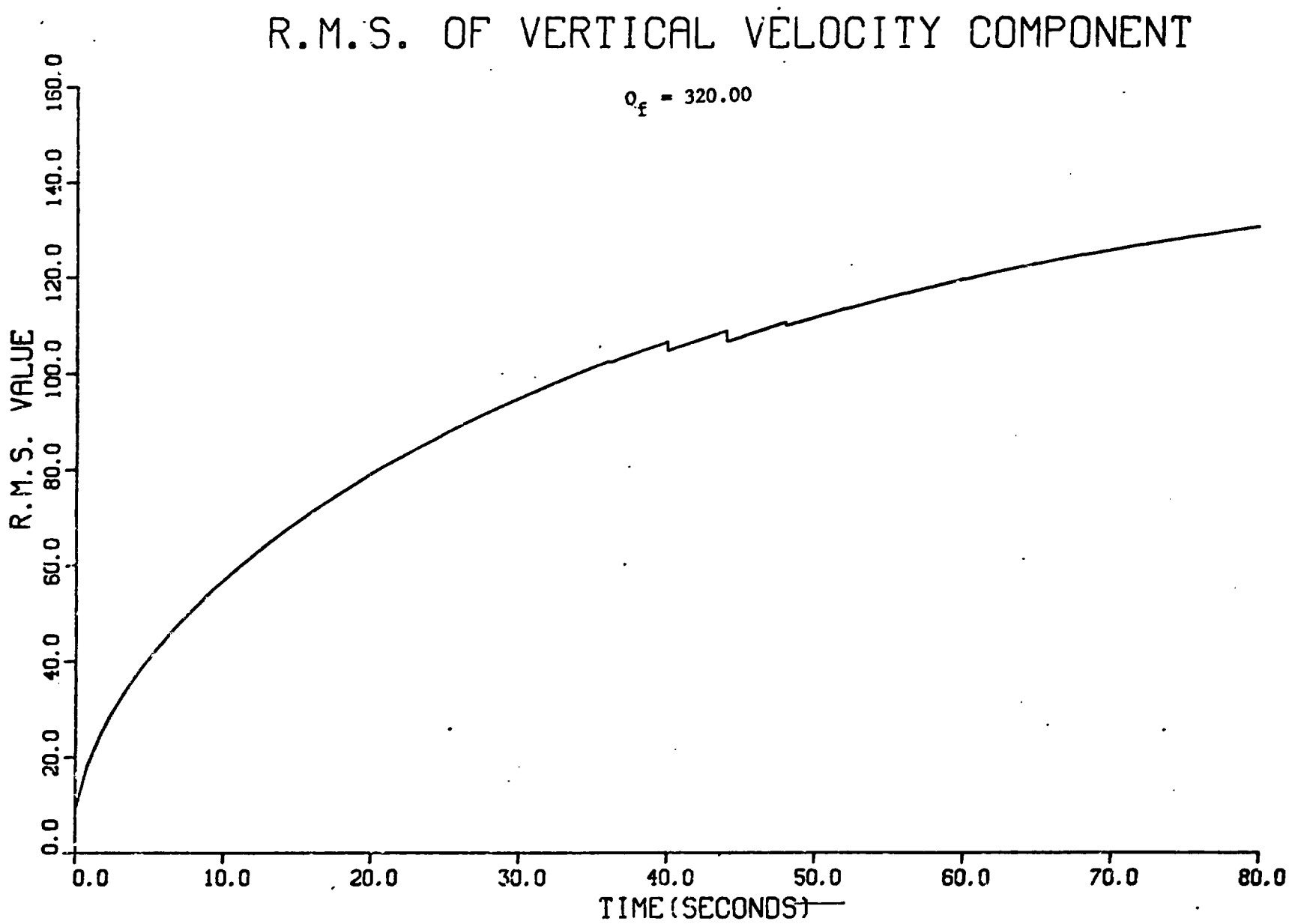

Figure 3-(c): R.M.S. OF VERTICAL VELOCITY COMPONENT FOR Q_f = 320.0

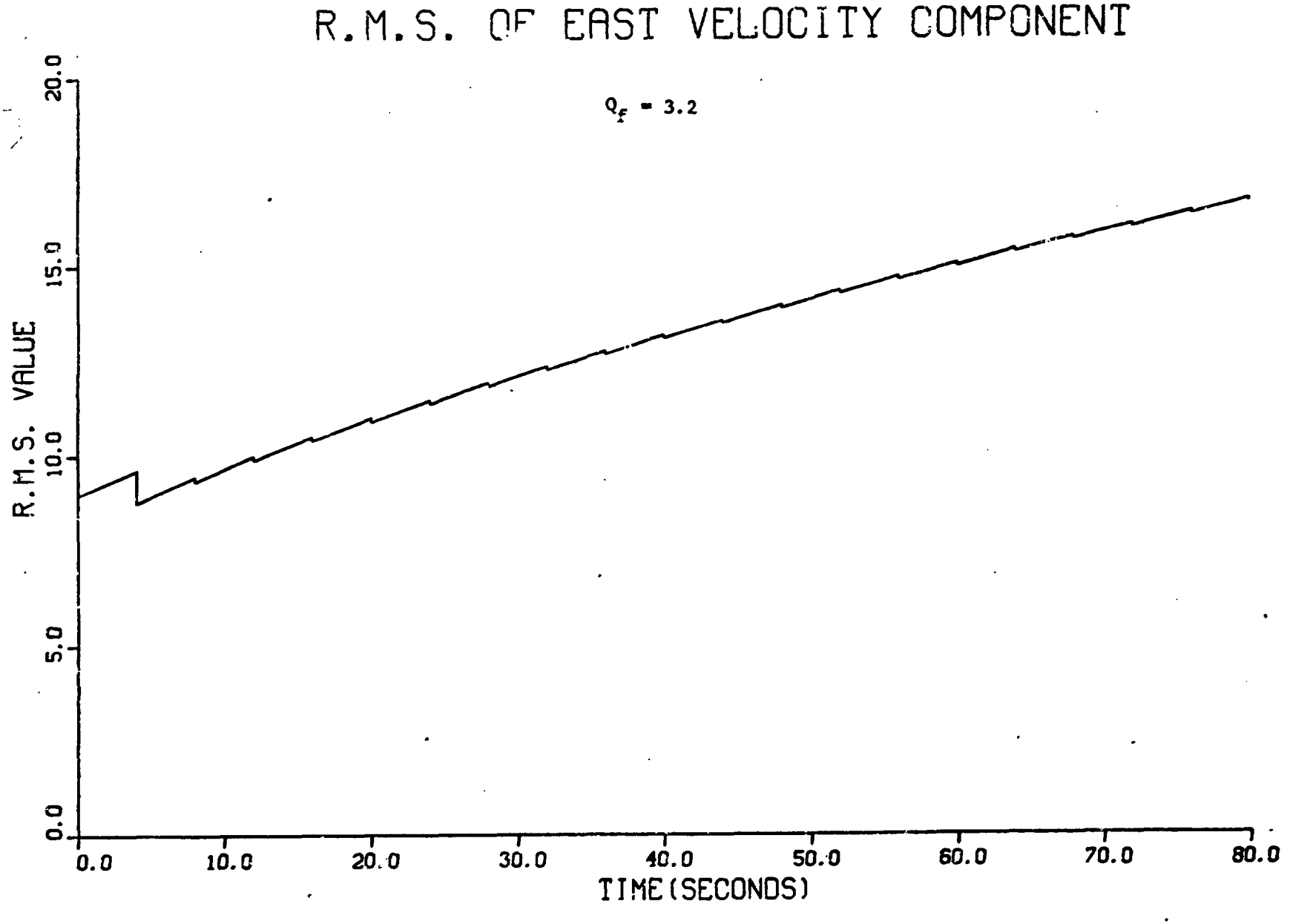

Figure 4-(a): R.M.S. OF EAST VELOCITY COMPONENT FOR Q_f = 3.2

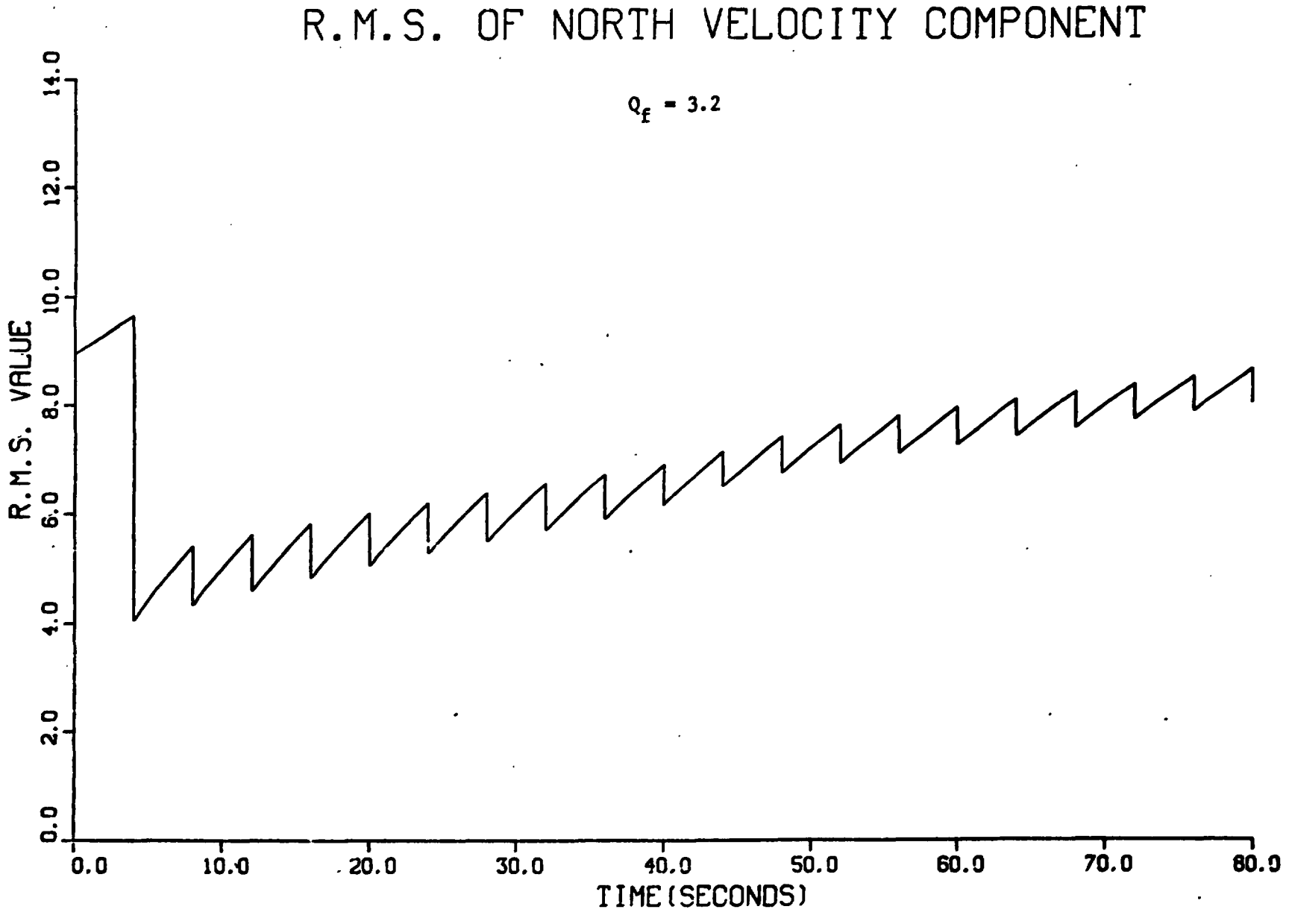

Figure 4-(b): R.M.S. OF NORTH VELOCITY COMPONENT FOR Q_f = 3.2

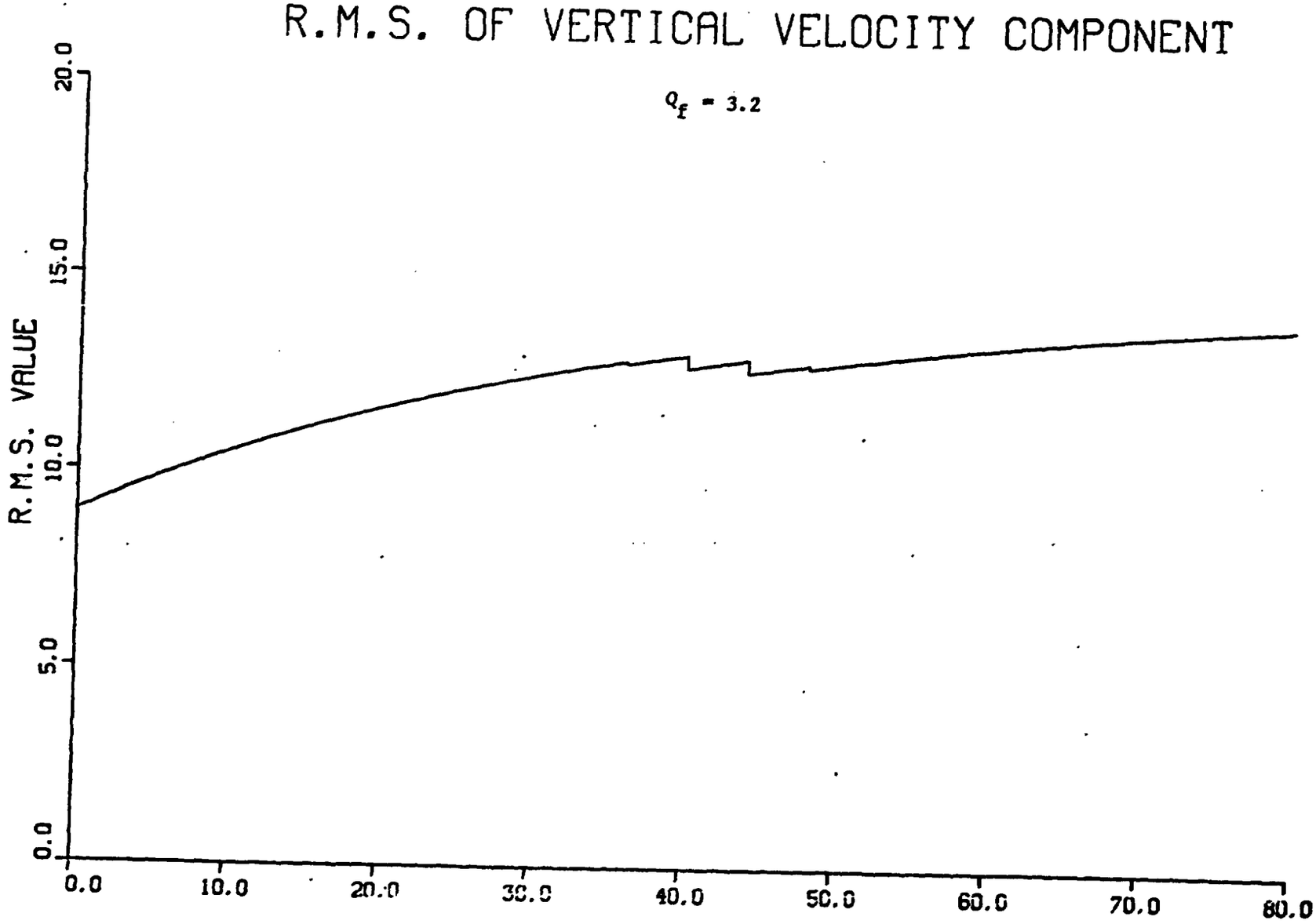

Figure 4-(c): R.M.S. OF VERTICAL VELOCITY COMPONENT OF Q_f = 3.2

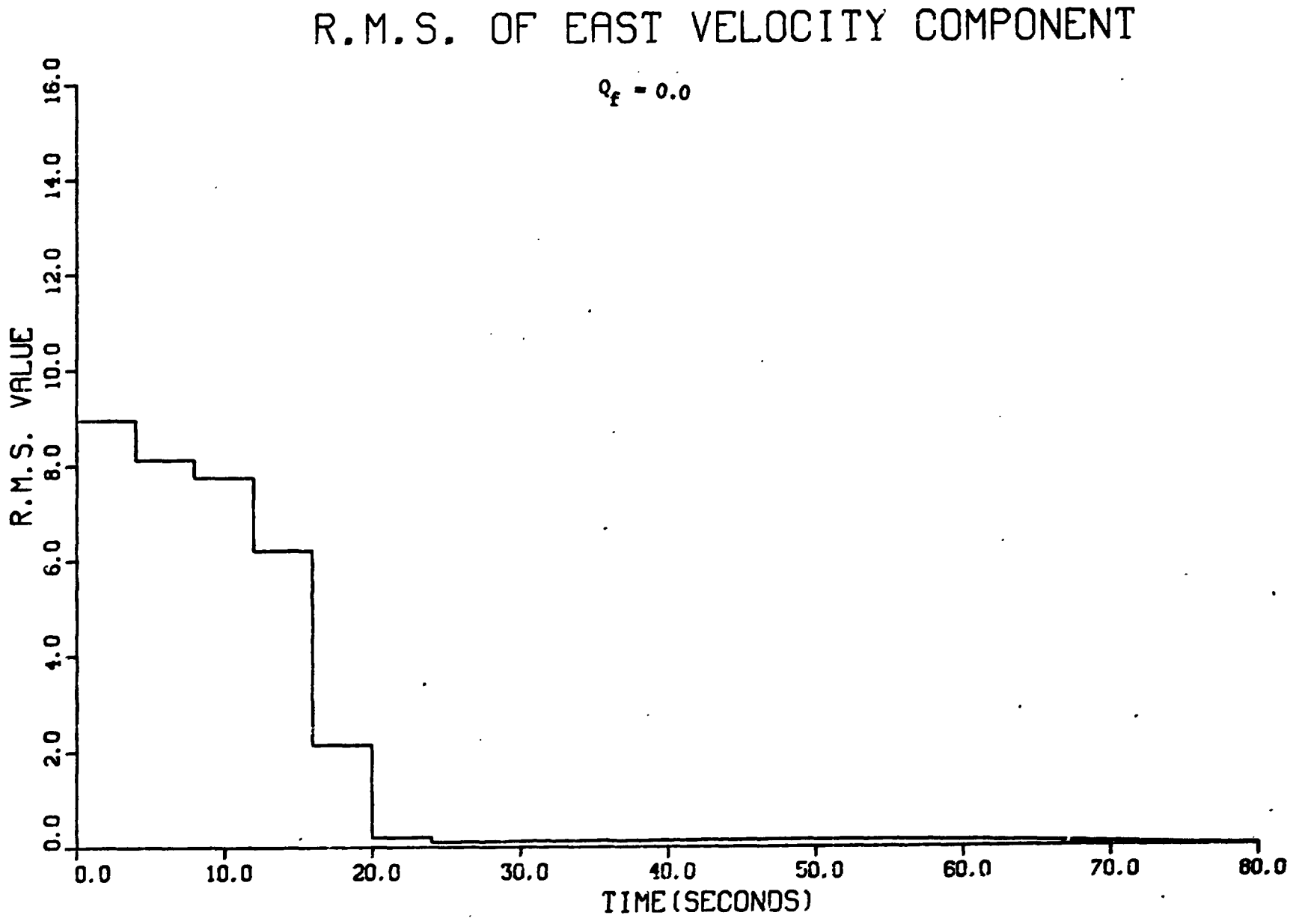

Figure 5-(a): R.M.S. OF EAST VELOCITY COMPONENT FOR Q_f = 0.0

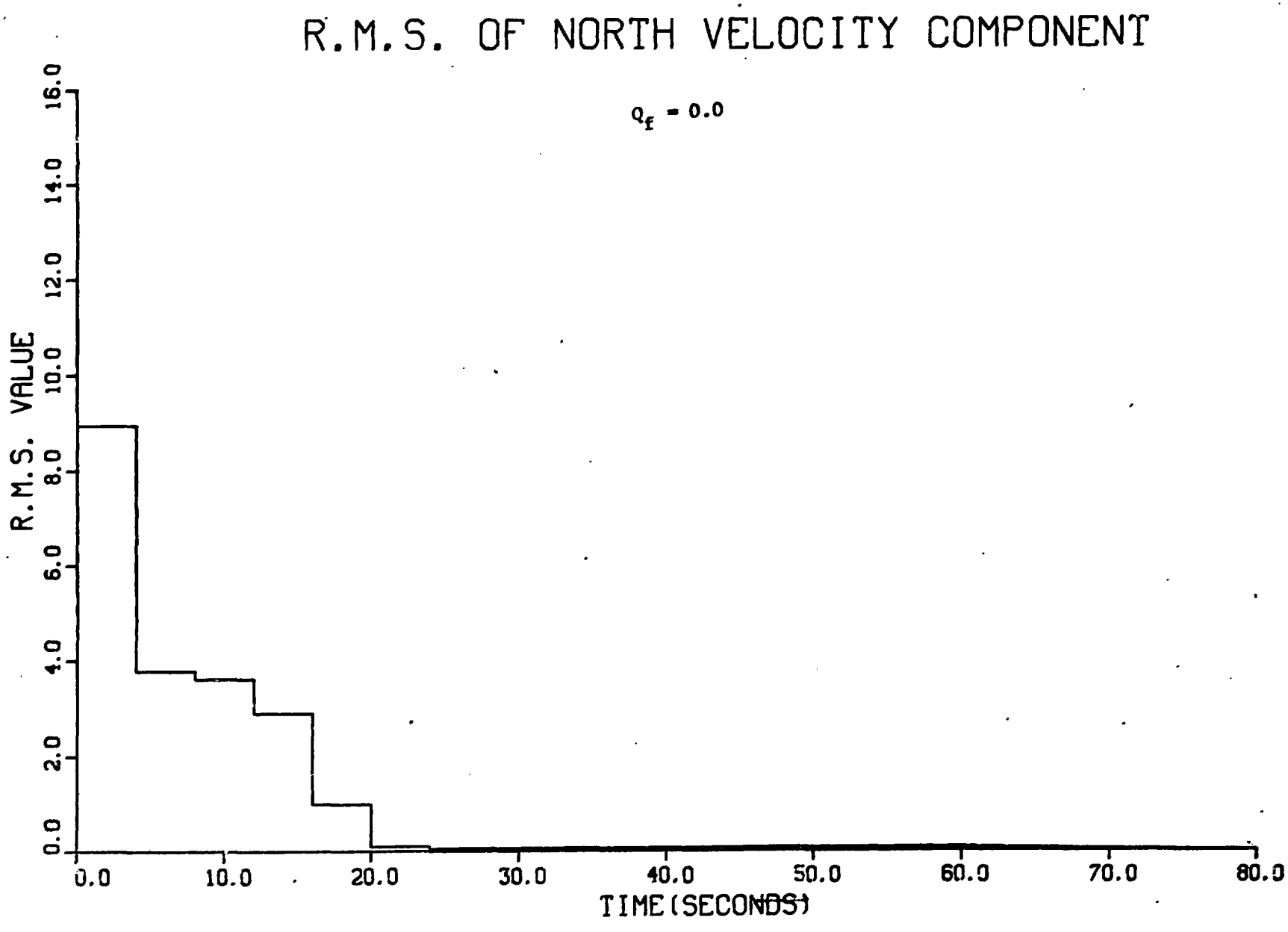

Figure 5-(b): R.M.S. OF NORTH VELOCITY COMPONENT FOR Q_f = 0.0

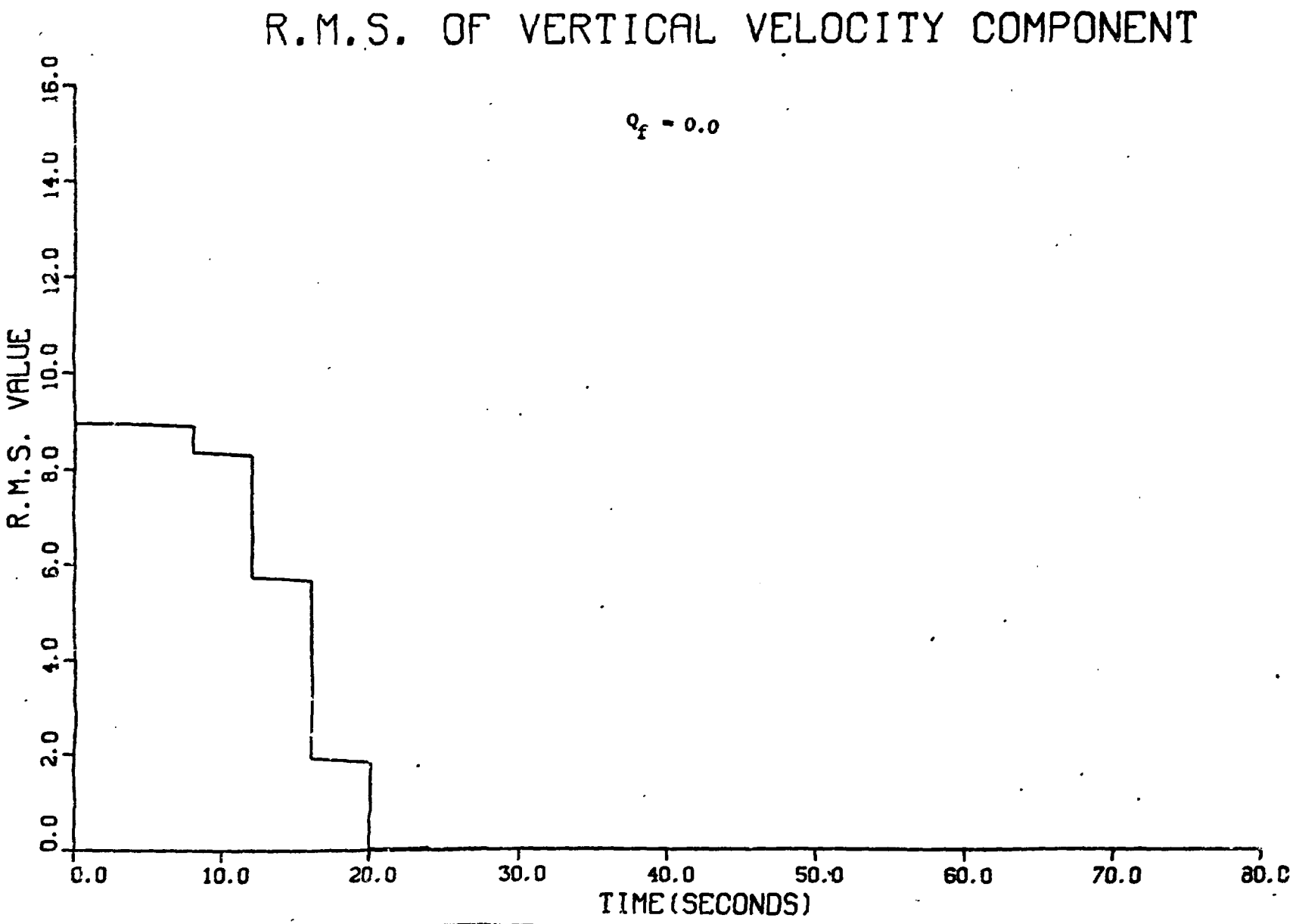

Figure 5-(c): R.M.S. OF VERTICAL VELOCITY COMPONENT FOR Q_f = 0.0

APPENDIX I

LN-15

TRUTH STATE INDEX	ERROR SOURCE	ERROR MODEL
1	EAST LONGITUDE	DYNAMIC
2	NORTH LATITUDE	DYNAMIC
3	ALTITUDE	DYNAMIC
4	EAST VELOCITY	DYNAMIC
5	NORTH VELOCITY	DYNAMIC
6	VERTICAL VELOCITY	DYNAMIC
7	EAST ATTITUDE	DYNAMIC
8	NORTH ATTITUDE	DYNAMIC
9	VERTICAL ATTITUDE	DYNAMIC
10	VERTICAL ACCELERATION	DYNAMIC
11	X GYRO DRIFT	RANDOM WALK
12	Y GYRO DRIFT	RANDOM WALK
13	Z GYRO DRIFT	RANDOM WALK
14	X GYRO G-SENS DRIFT. INPUT(X)	RANDOM CONSTANT
15	X GYRO G-SENS DRIFT, SPIN(Y)	RANDOM CONSTANT
16	Y GYRO G-SENS DRIFT, SPIN(X)	RANDOM CONSTANT
17	Y GYRO G_SENS DRIFT, INPUT(Y)	RANDOM CONSTANT
18	Z GYRO G-SENS DRIFT, SPIN(Y)	RANDOM CONSTANT
19	Z GYRO G-SENS DRIFT, INPUT(Z)	RANDOM CONSTANT
20	X GYRO G*G-SENS DRIFT	RANDOM CONSTANT
21	Y GYRO G*G-SENS DRIFT	RANDOM CONSTANT
22	Z GYRO G*G-SENS DRIFT	RANDOM CONSTANT
23	X GYRO SCALE FACTOR	RANDOM CONSTANT
24	Y GYRO SCALE FACTOR	RANDOM CONSTANT
25	Z GYRO SCALE FACTOR	RANDOM CONSTANT
26	X GYRO MISALIGNMENT ABT Y	RANDOM CONSTANT
27	X GYRO MISALIGNMENT ABT Z	RANDOM CONSTANT
28	Y GYRO MISALIGNMENT ABT X	RANDOM CONSTANT
29	Y GYRO MISALIGNMENT ABT Z	RANDOM CONSTANT
30	Z GYRO MISALIGNMENT ABT X	RANDOM CONSTANT
31	Z GYRO MISALIGNMENT ABT Y	RANDOM CONSTANT
32	X ACCELEROMETER BIAS	RANDOM WALK
33	Y ACCELEROMETER BIAS	RANDOM WALK
34	Z ACCELEROMETER BIAS	RANDOM WALK
35	X ACCELEROMETER SCALE FACTOR	RANDOM CONSTANT
36	Y ACCELEROMETER SCALE FACTOR	RANDOM CONSTANT
37	Z ACCELEROMETER SCALE FACTOR	RANDOM CONSTANT
38	X ACCEL MISALIGNMENT ABT Y	RANDOM CONSTANT
39	X ACCEL MISALIGNMENT ABT Z	RANDOM CONSTANT
40	Y ACCEL MISALIGNMENT ABT X	RANDOM CONSTANT
41	Y ACCEL MISALIGNMENT ABT Z	RANDOM CONSTANT
42	Z ACCEL MISALIGNMENT ABT X	RANDOM CONSTANT
43	Z ACCEL MISALIGNMENT ABT Y	RANDOM CONSTANT
44	BARD ALTIMETER BIAS	FIRST ORDER MARKOV
45	EAST ACCELERATION	
46	NORTH ACCELERATION	
47	VERTICAL ACCELERATION	

FILTER STATE INDEX	ERROR SOURCE	ERROR MODEL
1	EAST LONGITUDE	DYNAMIC
2	NORTH LATITUDE	DYNAMIC
3	ALTITUDE	DYNAMIC
4	EAST VELOCITY	DYNAMIC
5	NORTH VELOCITY	DYNAMIC
6	VERTICAL VELOCITY	DYNAMIC
7	EAST ATTITUDE	DYNAMIC
8	NORTH ATTITUDE	DYNAMIC
9	VERTICAL ATTITUDE	DYNAMIC
10	BARO ALTIMETER BIAS	FIRST ORDER MARKOV
11	X GYRO DRIFT	RANDOM WALK
12	Y GYRO DRIFT	RANDOM WALK
13	Z GYRO DRIFT	RANDOM WALK
14	AZIMUTH MEASUREMENT BIAS	FIRST ORDER MARKOV
15	ELEVATION MEASUREMENT BIAS	FIRST ORDER MARKOV

APPENDIX II

It is of interest to analytically investigate the observability of Case (A). Inasmuch as the F matrix of the LN-15 is far too complicated to be analytically tractable, a second-order system is instead analyzed using the nonlinear measurement, $X_1^2 + X_2^2$.

Consider the invariant, linear system given by

$$\ddot{x} + k_1\dot{x} + k_2 x = f(t) \tag{A.2.1}$$

which, in state variable form, becomes

$$\begin{bmatrix}\dot{x}_1\\ \dot{x}_2\end{bmatrix} = \begin{bmatrix}0 & \underline{F} & 1\\ -k_2 & & -k_1\end{bmatrix}\begin{bmatrix}x_1\\ x_2\end{bmatrix} + \begin{bmatrix}0\\ f(t)\end{bmatrix} \tag{A.2.2}$$

where the measurement, , is now

$$= x_1^2 + x_2^2 \tag{A.2.3}$$

or

$$\underline{H}^T = \begin{bmatrix}2x_1\\ 2x_2\end{bmatrix} \tag{A.2.4}$$

for the extended filter. Using expression (13), we have for the observability matrix, Φ,

$$\Phi = \begin{bmatrix}2x_1 & -2k_2x_2\\ 2x_2 & 2x_1 - 2k_1x_2\end{bmatrix} \tag{A.2.5}$$

with a determinant equal to

$$x_1^2 - k_1 x_1 x_2 + x_2^2 \tag{A.2.6}$$

which provides the following condition for nonobservability,

$$x_1^2 - k_1 x_1 x_2 + x_2^2 = (x_1 - c_1 x_2)(x_1 - c_2 x_2) = 0 \tag{A.2.7}$$

Nonobservable regions of (x_1, x_2) space (other than origin) are the straight lines, $x_1 - c_1 x_2$, if and only if c_1, c_2 are real numbers which correspond to the overdamped case which of course describe the F matrix of the highly overdamped LN-15 INS. Observability with the "Auto-Focus" update will be further complicated by the sparseness of the LN-15 F matrix and the fact that the measurement involves only a subset of state AF variables.

In summary, the above analogy does suggest that the AF update may well have serious observability problems.

APPENDIX B

Centripedal Acceleration Only

TMEAS = 8.0 ; Autofocus (N_e); Compass (N_o); Vertical Doppler (N_d)

TMEASI = 48 ; QF = 320 .

Update Number No.	Longitude 1	Latitude 2	Altitude 3	East Velocity 4	North Velocity 5	Vertical Velocity 6	East Attitude 7	North Attitude 8	Vertical Attitude 9
1	75	100	133	71	42	115	92	96	100
2	74	82	125	69	36	115	89	95	100
3	73	70	120	68	31	115	86	94	100
4	72	61	124	66	28	115	83	93	100
5	71	54	116	65	25	115	80	92	100
6	70	49	115	64	23	114	71	91	100
7	69	44	115	63	22	114	73	90	100
8	68	41	113	62	21	114	70	89	100
9	67	38	113	61	20	114	66	88	100
10	66	36	112	60	19	114	63	87	100
11	65	34	111	60	19	114	59	85	100
12	65	32	109	59	18	113	56	84	100
13	64	31	108	59	17	113	52	83	100
14	63	30	108	58	17	113	49	82	100
15	63	28	108	57	16	113	47	80	100
16	62	28	107	57	16	113	44	79	101
17	61	27	108	56	17	114	41	78	101
18	61	26	109	55	17	115	39	77	101
19	60	25	109	55	17	116	37	75	101
20	60	25	110	54	17	117	35	74	101
	M=64 σ=11.4	M=43 σ=21	M=114 σ=7.6	M=61 σ=4.94	M=22 σ=7.2	M=115 σ=1.0			

TABLE (B2).

Centripedal Acceleration Only

TMEAS = 8.0; Autofocus (γ_{eb}); Compass (γ_{eb}); Vertical Doppler (N_d)

TMEASI = 48; QF = 320.

Update Number No.	Longitude 1	Latitude 2	Altitude 3	East Velocity 4	North Velocity 5	Vertical Velocity 6	East Attitude 7	North Attitude 8	Vertical Attitude 9
1	13	10	132	0.095	35	115	96	88	101
2	4	25	128	40	60	115	93	82	101
3	7	20	125	64	25	116	93	76	101
4	11	15	119	13	15	115	89	77	101
5	7	19	116	30	48	115	87	75	101
6	6	20	116	14	13	115	86	70	101
7	5	20	115	5	26	115	83	68	101
8	7	17	114	35	2	115	81	64	101
9	10	13	113	45	9	115	78	63	101
10	10	13	112	6	24	115	74	62	102
11	13	10	111	58	17	115	72	58	102
12	15	8	109	17	8	114	65	57	102
13	15	8	108	21	5	114	62	54	102
14	15	7	108	21	4	114	60	52	102
15	15	6	109	18	5	115	58	51	102
16	16	6	110	20	3	116	56	49	102
17	15	6	110	2	12	117	53	48	102
18	13	7	110	12	20	117	51	46	102
19	12	7	111	2	11	118	51	42	102
20	12	7	111	11	5	119	50	40	102
	M=11 σ=11	M=11 σ=	M=115 σ=2	M=21 σ=4.55	M=16 σ=16	M=116 σ=1.5			

TABLE (B3)

Centripedal Acceleration Only

TMEAS = 8.0; Autofocus (No); Compass (Yes); Vertical Doppler (No)

TMEASI = 48; QF 320.

Update Number No.	Longitude 1	Latitude 2	Altitude 3	East Velocity 4	North Velocity 5	Vertical Velocity 6	East Attitude 7	North Attitude 8	Vertical Attitude 9
1	38	211	99	28	178	100	104	91	100
2	36	199	99	32	166	100	105	89	100
3	30	197	99	9	198	99	107	87	101
4	35	183	100	98	102	100	109	84	101
5	40	176	100	48	145	100	109	84	101
6	37	174	99	6	175	99	110	83	101
7	37	170	100	51	139	100	113	80	101
8	38	168	100	32	151	100	114	79	101
9	40	162	100	74	121	100	116	76	101
10	44	155	100	65	112	100	116	76	101
11	45	155	100	34	147	100	116	77	101
12	49	152	100	100	106	100	119	74	101
13	52	152	100	68	129	100	119	76	101
14	53	150	100	61	133	100	120	76	101
15	54	148	100	65	129	100	120	75	101
16	55	146	100	66	128	100	121	74	101
17	56	144	100	64	128	100	121	74	101
18	56	143	100	66	127	100	121	73	101
19	56	143	100	49	136	100	121	73	101
20	55	143	100	34	144	100	121	72	101
	M=45 σ=8.3			M=34 σ=26	M=141 σ=27	M=100 σ=1			

TABLE (B4)

Centripedal Acceleration Only

TMEAS = 8.0 ; Autofocus (Yes); Compass (Yes); Vertical Doppler (Yes)

TMEASI = 48 ; QF 320 .

Update Number No.	Longitude 1	Latitude 2	Altitude 3	East Velocity 4	North Velocity 5	Vertical Velocity 6	East Attitude 7	North Attitude 8	Vertical Attitude 9
1	8	27	113	5	9	1	95	88	101
2	6	17	72	2	5	1	93	85	101
3	0.69	4	95	46	[illegible]	1	91	81	101
4	2	7	70	59	47	1	90	77	101
5	6	10	34	8	3	1	86	76	101
6	2	5	17	35	29	1	83	73	101
7	1	3	15	8	3	1	81	69	101
8	0.35	2	7	10	9	1	78	66	101
9	2	3	6	30	18	1	76	62	101
10	5	6	0.171	40	24	2	72	61	102
11	5	5	6	11	9	2	68	60	102
12	8	8	17	53	31	2	66	56	102
13	10	9	25	20	10	2	61	56	102
14	10	8	28	12	5	2	58	54	102
15	10	8	28	16	7	1	55	52	102
16	11	8	28	16	7	2	53	50	102
17	11	8	24	14	6	0.73	50	48	102
18	11	8	18	16	7	0.981	48	46	102
19	10	8	13	1	3	1.5	46	45	102
20	9	6	15	15	11	2	44	43	102

CONTINUED

Centripedal Acceleration Only

TMEAS = 8.0 ; Autofocus (Ye) Compass (ea); Vertical Doppler (ed)

TMEASI = 48 ; QF 320 .

Update Number No.	Longitude 1	Latitude 2	Altitude 3	East Velocity 4	North Velocity 5	Vertical Velocity 6	East Attitude 7	North Attitude 8	Vertical Attitude 9
21	8	6	13	1	3	1	43	39	102
22									
23	8	5	13	8	2	2	42	37	102
24	7	5	18	6	5	3	40	36	103
25	7	5	27	20	8	4	40	32	103
26	7	5	31	11	3	3	38	31	103
27	7	5	36	9	2	3	37	30	103
28	6	4	42	21	13	4	35	30	103
29	6	4	45	7	1	3	36	26	103
30	5	3	47	17	11	3	34	26	103
31	3	2	50	23	14	4	34	25	103
32	1	1	53	34	20	5	34	23	103
33	1	1	54	3.0	0.391	2.0	35	19	104
34	0.06	0.197	54	29	17	3	34	20	104
35	0.71	0.57	56	14	5	3	35	16	104
36	1	0.76	58	9	3	5	35	16	104
37	0.71	0.58	59	7	4	2	34	17	104
	M=5.46 σ=3.66	M=7.0 σ=6.81	M=35 σ=27	M=17 σ=14	M=11 σ=12	M=2.22 σ=1.20			

Centripedal Acceleration Only

TMEAS = 8.0 ; Autofocus (Yes) Compass (Yes) Vertical Doppler (Yes)
Altitude (Yes)

TMEASI = 48 ; QF 320 .

Update Number No.	Longitude 1	Latitude 2	Altitude 3	East Velocity 4	North Velocity 5	Vertical Velocity 6	East Attitude 7	North Attitude 8	Vertical Attitude 9
1	8	27	11	5.2	9	1	95	88	101
2	6	17	5.5	3	5.7	1	93	85	101
3	.6	4.7	5.7	46	44	2	91	81	101
4	2.8	7.9	.8	59.5	47	1.7	90	77	101
5	6.2	10	2.8	8.1	4.0	1.55	86.5	76.5	101
6	1.17	3.5	1.6	8.7	4.0	1.4	82	69	101
7	.3	2.2	1.6	10.6	1.6	1.6	79	67	101
8	2.2	3.7	.7	30	18	1.6	76	62	102
9	5.89	6.63	4.5	41	25	2.1	73	61	102
10	5.5	5.9	2.7	11.4	9.7	3.0	68	61	102
11	8.3	8.0	3.3	53	32	2.9	66	56	102
12	10.0	9.0	5.6	20.2	10.3	3.17	62	56	102
13	10.3	9.0	4.1	12.6	5.5	2.8	58	55	102
14	10.7	9.0	1.8	16.5	7.7	2.2	56	52	102
15	11.0	9.0	0.57	15.6	7.5	3.0	53	50	102
16	11.3	9.0	1.19	14.6	6.3	1.4	51	49	102
17	11.6	8.8	.28	16.2	7.17	1.45	49	47	102
18	10.7	8.1	2.5	1.33	2.92	1.8	46.1	45.3	102
19	9.0	6.7	2.4	15.8	11.0	3.0	44.3	43.3	102
20	8.19	6.0	2.8	1.17	2.34	2.07	43.6	39.81	103

CONTINUED

Centripedal Acceleration Only

TMEAS = 8.0 ; Autofocus (Yes); Compass (Yes) Vertical Doppler (Yes)
Altitude (Yes)

TMEASI = 48 ; QF 320 .

Update Number No.	Longitude 1	Latitude 2	Altitude 3	East Velocity 4	North Velocity 5	Vertical Velocity 6	East Attitude 7	North Attitude 8	Vertical Attitude 9
21	8.0	5.8	.75	8.6	2.6	3.14	42.5	37.0	102
22	7.19	5.12	5.16	6.8	5.9	4.0	41	36	103
23	7.75	5.40	7.28	20.50	8.90	5.22	40.4	32.5	103
24	7.9	5.42	2.44	11.07	3.77	4.38	30.6	31.9	103
25	7.9	5.36	6.53	9.24	2.98	5.23	37.6	30.8	103
	M=7.14 σ=23.41	M=7.66 σ=22.76	M=3.34 σ=2.57	M=17.5 σ=15.9	M=11.41 σ=12.46	M=23.3 σ=23.64			

TABLE (B6)

Centripedal Acceleration Only

TMEAS = 8; Autofocus (No); Compass (Yes); Vertical Doppler (Yes)

TMEASI = 48; QF 320 Altitude(Yes).

Update Number No.	Longitude 1	Latitude 2	Altitude 3	East Velocity 4	North Velocity 5	Vertical Velocity 6	East Attitude 7	North Attitude 8	Vertical Attitude 9
1	38	211	12	28	179	1.10	104	91	100
2	36	199	5.6	32.4	167	1.0	106	89	100
3	35	183	.8	98	102	1.7	109	84	101
4	41	177	2.8	48	146	1.5	109	85	101
5	37	174	.2	6.1	175	1.2	110	83	101
6	37	171	1.5	51	139	1.4	113	80	101
7	38	168	1.6	33	152	1.6	114	79	101
8	41	162	.7	74	122	1.7	116	77	101
9	45	156	4.5	86	113	2.1	117	76	101
10	45	156	2.6	34	147	3.0	117	78	101
11	50	152	3.0	100	106	2.8	119	75	101
12	53	153	5.6	69	130	3.15	120	77	101
13	54	151	4.1	61	133	2.75	120	76	101
14	55	149	1.76	66	130	2.16	121	75	101
15	56	147	.57	66	129	2.99	121	75	101
16	56	145	1.2	65	129	1.39	122	74	101
17	57	143	.279	66	127	1.4	121.8	74	101
18	55	143	2.46	35	144	2.9	122	73	101
19	55	143	2.8	49	135	2.0	123	70	101
20	55	141	.75	60	128	3.0	124	68	101
	M=44 σ=14.2	M=161 σ=19.2	M=2.74 σ=2.74	M=56 σ=24	M=132 σ=32	M=2.0 σ=0.74			

Centripedal Acceleration Only

TMEAS = 8.0 ; Autofocus (NO); Compass (Y); Vertical Doppler (Y)

TMEASI = 48 ; QF 320 .

Update Number No.	Longitude 1	Latitude 2	Altitude 3	East Velocity 4	North Velocity 5	Vertical Velocity 6	East Attitude 7	North Attitude 8	Vertical Attitude 9
1	1	210	109	28	178	1.3	104	92	100
2	36	199	42	32	166	1.1	105	89	100
3	31	197	40	9	198	2.2	107	87	101
4	35	180	10	97	100	1.7	109	84	101
5	37	170	35	5	172	1.0	110	83	101
6	36	165	40	50	135	1.0	112	79	101
7	36	162	47	31	147	1.0	113	78	101
8	39	156	50	72	117	1.0	114	76	101
9	43	149	55	84	109	1.3	115	75	101
10	44	149	59	33	143	2	114	76	101
11	47	142	64	98	99	1.6	116	73	101
12	50	140	68	65	120	1.7	115	75	101
13	51	137	71	62	121	0.259	116	73	101
14	52	135	72	63	121	0.900	116	72	101
15	53	134	71	61	121	0.789	116	72	101
16	53	133	69	63	120	0.705	116	72	101
17	53	133	67	46	130	0.233	116	72	101
18	52	134	67	32	138	0.785	117	70	101
19	52	134	66	47	129	0.317	118	68	101
20	52	132	65	57	123	0.813	118	66	101

TABLE (37)
Continued

Centripedal Acceleration Only

TMEAS =_____; Autofocus ( ); Compass ( ); Vertical Doppler ( )

TMEASI =_____; QF_____.

Update Number No.	Longitude 1	Latitude 2	Altitude 3	East Velocity 4	North Velocity 5	Vertical Velocity 6	East Attitude 7	North Attitude 8	Vertical Attitude 9
21	51	133	66	42	131	1.59	118	66	101
	M=45	M=.53	M=58.7	M=51	M=134	M=1.10			
	σ=7.7	σ=25	σ=20	σ=25	σ=26	σ=0.54			

TABLE (B8)

Centripedal Acceleration Only

TMEAS = 4.0 ; Autofocus (Yes); Compass (Yes); Vertical Doppler (Yes)

TMEASI = 48 ; QF 320 .

Update Number No.	Longitude 1	Latitude 2	Altitude 3	East Velocity 4	North Velocity 5	Vertical Velocity 6	East Attitude 7	North Attitude 8	Vertical Attitude 9
2				58	59	1.2			
4				7.9	7.2	1.2			
6				9.8	6.4	0.5			
8				29	22	0.58			
10				0.207	1.2	1.0			
12				7.5	5.2	1.4			
14				8.5	6.19	.687			
16				0.254	0.883	1.01			
18				7.53	3.34	1.45			
20				5.3	2.03	1.6			
22				10.1	6.6	1.3			
24				12.1	5.6	1.5			
26				8.8	3.8	1.18			
				M=12 σ=15	M=10 σ=16	M=1.12 σ=0.35			

TABLE (B9)

Centripedal Acceleration Only

TMEAS = 16.0 ; Autofocus (Ye) Compass (Ye) Vertical Doppler (Ye)

TMEASI = 48 ; QF 320 .

Update Number No.	Longitude 1	Latitude 2	Altitude 3	East Velocity 4	North Velocity 5	Vertical Velocity 6	East Attitude 7	North Attitude 8	Vertical Attitude 9
1				3.3	4.8	.69			
2				76	57	.33			
3				29	22	1.13			
4				1.01	.398	1.56			
5				54	35	1.2			
6				40	26	1.6			
7				2.8	.737	.969			
8				10.0	4.83	1.03			
9				2.21	2.20	.99			
10				24	14	1.3			
11				13.1	6.3	1.3			
12				5.7	2.2	.96			
13				4.8	1.6	1.5			
14				11.3	5.1	1.15			
15				7.78	5.07	1.66			
16				3.17	2.63	.18			
17				19	11.	.95			
				M=18 σ=21	M=12 σ=15	M=1.09 σ=0.41			

TABLE (B10)

Centripedal Acceleration Only

TMEAS = 8.0 ; Autofocus (Yes); Compass (Yes); Vertical Doppler (Yes)

TMEASI = 1048.0 ; QF 3.2 .

Update Number No.	Longitude 1	Latitude 2	Altitude 3	East Velocity 4	North Velocity 5	Vertical Velocity 6	East Attitude 7	North Attitude 8	Vertical Attitude 9
1	46	23	129	74	3	20	82	74	100
2	45	23	134	92	6	8	97	94	100
3	115	79	140	589	379	15	170	39	99
4	7	6	230	75	35	17	80	111	99
5	57	37	289	245	237	9	188	11	99
6	29	15	590	62	35	11	54	114	99
7	40	26	3629	58	73	10	114	53	99
8	1	5	402	172	145	10	47	178	99
9	29	15	590	62	35	11	54	114	99
10	40	26	3629	58	73	10	114	53	99
11	1	5	402	172	145	10	47	178	99
12	5	9	25	46	67	16	138	11	99
13	57	48	12	239	227	15	367	413	101
14	51	46	26	78	105	10	11	101	94
15	50	46	28	60	39	8	49	34	95
16	51	47	27	59	59	6	107	41	93
17	51	50	23	43	82	0.15	5	62	94
18	51	52	7	54	64	0.097	117	26	92
19	48	48	8	10	9	0.102	56	194	92
20	38	42	9	62	45	0.749	192	1118	91

CONTINUED

Centripedal Acceleration Only

TMEAS = 8.0 ; Autofocus ( ); Compass ( ); Vertical Doppler ( )

TMEASI = 1048.0 ; QF 3.2 .

Update Number No.	ngitude 1	Latitude 2	Altitude 3	East Velocity 4	North Velocity 5	Vertical Velocity 6	East Attitude 7	North Attitude 8	Vertical Attitude 9
21	31	35	10	9	3	0.325	1060	3554	86
22	29	32	19	28	9	0.653	1398	2104	86
23	25	29	7	30	10	0.945	922	5713	88
24	26	27	14	73	24	1.687	1804	450	87
25	28	27	28	37	12	1.03	1406	1967	88
26	28	25	35	30	9	1.35	1219	2133	88
27	23	22	45	84	28	2	333	7735	89
28	20	20	50	21	6	1	993	1838	90
29	16	18	52	70	23	1	378	5516	90
30	10	15	55	94	31	1.8	239	5919	91
31	2	11	58	133	44	2.6	33	6645	92
32	0.176	10	60	7	2	0.931	754	1310	92
33	4	8	60	112	37	1	145	4946	93
34	4	8	61	46	15	1	872	120	93
35	2	8	63	29	9	3	752	381	93
36	2	7	65	27	9	2	474	1885	94
37	3.2	7	67	6	2	3	544	1224	94
38	3.2	7	67	5	2	5	536	1206	94

TABLE (B11)

Centripedal Acceleration Only

TMEAS = 8.0 ; Autofocus (yes); Compass (yes); Vertical Doppler (yes)

TMEASI = 1048.0 ; QF 0.0032 .

Update Number No.	Longitude 1	Latitude 2	Altitude 3	East Velocity 4	North Velocity 5	Vertical Velocity 6	East Attitude 7	North Attitude 8	Vertical Attitude 9
1	46	23	126	73	3	20	104	105	100
2	44	23	133	91	6	8	102	103	100
3	116	80	140	586	378	16	101	104	101
4	3	15	161	575	413	18	102	103	100
5	6	6	228	75	35	17	103	103	100
6	57	37	287	244	236	9	103	104	100
7	28	15	586	62	34	11	103	104	100
8	40	26	3601	57	73	10	104	105	100
9	0.76	6	399	171	144	10	105	105	100
10	31	32	158	213	188	10	108	105	100
11	5	9	25	45	67	15	111	105	100
12	57	48	13	237	224	16	117	108	100
13	51	47	26	77	104	9	111	103	100
14	50	46	28	60	38	9	126	106	100
15	51	47	28	60	58	6	127	107	100
16	51	47	28	60	58	6	127	107	100
17	51	50	24	43	82	0.163	115	104	100
18	51	52	7	54	64	0.076	129	107	100
19	48	49	8	10	9	0.032	137	107	100
20	36	42	8	62	45	0.439	200	118	100

CONTINUED

Centripedal Acceleration Only

TMEAS = 8.0 ; Autofocus ( ); Compass ( ); Vertical Doppler ( )

TMEASI = 1048.0 ; QF 0.0032 .

Update Number No.	Longitude 1	Latitude 2	Altitude 3	East Velocity 4	North Velocity 5	Vertical Velocity 6	East Attitude 7	North Attitude 8	Vertical Attitude 9
21	31	35	10	9	3	0.317	95	36	101
22	29	32	19	28	9	0.638	103	96	101
23	25	29	7	30	10	0.928	120	122	101
24	26	28	14	73	24	1	116	252	101
25	28	27	29	37	12	1	118	235	101
26	28	25	35	39	9	1	106	199	101
27	23	22	45	84	28	2	100	123	101
28	20	20	50	21	6	1.5	80	180	102
29	16	18	52	70	24	1.5	77	129	102
30	10	15	55	93	31	1.8	68	130	102
31	2	12	59	133	45	2.6	60	129	102
32	10	15	55	93	31	1.8	68	130	102
33	2	12	59	133	45	2.6	60	129	102
34	0.188	10	60	7	1.6	0.935	44	188	103
35	4.6	8	60	111	37	1.22	45	141	103
36	2.2	8	63	29	9	2	30	172	103
37	2.8	7.5	65	26	9	2	30	144	103
38	3.2	6.9	67	5	2.6	3	26	146	103
39	3.2	6.8	68	4.9	3.0	4.9	25	145	103
40									

TABLE (B12)

Centripedal Acceleration Only

TMEAS = 0.0 ; Autofocus (Yes); Compass (Yes); Vertical Doppler (No)
Altitude (Yes)

TMEASI = 48 ; QF 320 .

Update Number No.	Longitude 1	Latitude 2	Altitude 3	East Velocity 4	North Velocity 5	Vertical Velocity 6	East Attitude 7	North Attitude 8	Vertical Attitude 9
1	11	6	5	2	23	65	95	88	101
2	8	4	9	0.8	16	47	94	85	101
3	1.2	7.5	1.3	44	54	54	93	82	101
4	4.7	2.7	3.2	61	41	35	91	78	101
5	7.6	2.5	2.07	7.75	5.35	6.5	88	77	101
6	3.5	0.70	0.86	36	27	13	85	74	101
7	2.3	2.04	3.11	9.97	0.202	28	83	70	101
8	1.2	1.7	3.5	11.9	5.7	26	80	67	101
9	3	0.063	0.33	31	16	20	77	63	102
10	6.6	3.6	4.5	41	24	3.5	73	62	102
11	6.0	3.9	0.5	13	5.1	33	69	61	102
12	6.5	7.2	.185	51	39	53	66	57	102
13	10	9.0	2.8	18	17	51	62	56	102
14	10	10	1.0	9.9	13	59	58	55	102
15	10	10	0.3	15	13	41	55	52	102
16	11	11	1.6	14.8	12	43	52	50	102
17	11	11	1.3	14	7	6	50	48	102
18	11	10	1.9	17	4.5	32	476	46	102
19	10	9.2	4.7	0.5	5.20	30	45	45	102
20	6.7	8	.8	17	8.7	28	44	43	102
	M=7.1 σ=3.5	M=6.0 σ=3.7	M=2.36 σ=2.16	M=20 σ=17	M=16 σ=14	M=33 σ=18			

TABLE (B13)

L.O.S. and Centripedal Acceleration

TMEAS = 8; Autofocus (Y); Compass (No); Vertical Doppler (NO)

TMEASI = 1048; QF 320.

Update Number No.	Longitude 1	Latitude 2	Altitude 3	East Velocity 4	North Velocity 5	Vertical Velocity 6	East Attitude 7	North Attitude 8	Vertical Attitude 9
1	70	18	173	65	41	132	96	96	100
2	68	10	155	62	31	133	95	94	100
3	67	3	160	59	22	134	92	93	100
4	66	0.69	152	57	17	134	90	92	100
5	64	3	140	54	13	132	87	91	100
6	62	6	134	53	9	131	84	89	100
7	61	8	132	52	7	131	80	88	100
8	60	10	129	51	4.6	130	77	86	100
9	59	11	129	50	2.6	130	73	85	100
10	56	12	126	49	1.0	130	70	83	100
11	57	12	124	48	0.495	129	66	82	100
12	56	13	121	48	1.4	128	63	80	101
13	55	14	118	47	2.2	126	59	78	101
14	55	14	117	47	3.0	126	56	77	101
15	54	14	116	46	4	126	53	76	101
16	53	15	116	46	5	126	50	74	101
17	52	15	115	45	7	128	45	71	101
18	52	16	119	44	8	130	42	70	101
19	51	16	120	44	8	130	40	69	101
20	51	16	120	44	9	131	38	67	101

TABLE (B13)
Continued

L.O.S. and Centripedal Acceleration

TMEAS = 8 ; Autofocus (Y); Compass (NO); Vertical Doppler (NO)

TMEASI = 1048 ; QF 320 .

Update Number No.	Longitude 1	Latitude 2	Altitude 3	East Velocity 4	North Velocity 5	Vertical Velocity 6	East Attitude 7	North Attitude 8	Vertical Attitude 9
21	49	17	118	43	10	131	33	64	101
	M=58 σ=6.5	M=11 σ=4.7	M=131 σ=16.8	M=48 σ=11.8	M=9.8 σ=10	M=130 σ=2.5			

L.O.S. and Centripedal Acceleration

TMEAS = 8.0 ; Autofocus (Y); Compass (Y); Vertical Doppler (NO)

TMEASI = 1048 ; QF 320 .

Update Number No.	Longitude 1	Latitude 2	Altitude 3	East Velocity 4	North Velocity 5	Vertical Velocity 6	East Attitude 7	North Attitude 8	Vertical Attitude 9
1	30	151	153	20	136	117	102	90	100
2	26	129	127	18	104	120	101	88	101
3	21	135	135	19	155	117	102	85	101
4	19	85	117	67	16	132	100	80	101
5	22	77	123	22	49	126	98	80	101
6	19	79	123	16	96	122	96	78	101
7	16	68	120	21	38	126	95	73	101
8	15	64	120	3	54	125	93	71	101
9	15	52	118	38	9	128	90	67	101
10	17	42	118	47	2.5	129	87	65	101
11	17	42	120	0.132	44	125	83	65	101
12	18	32	115	58	15	128	81	60	101
13	20	29	115	28	12	125	76	61	101
14	20	27	115	20	17	125	73	59	102
15	20	24	115	24	13	125	70	57	102
16	20	22	115	23	11	125	67	55	102
17	19	20	115	21	12	116	65	53	102
18	19	18	117	22	9	128	62	51	102
19	19	18	119	5	21	129	60	50	102
20	17	19	119	8	30	128	58	48	102
	M=19 σ=3.5	M=58 σ=42	M=121 σ=9.0	M=24 σ=15	M=41 σ=46				

TABLE (B15)

L.O.S. and Centripedal Acceleration

TMEAS = 8.0 ; Autofocus (Y); Compass (Y); Vertical Doppler (Y)

TMEASI = 1048 ; QF 320 .

Update Number No.	Longitude 1	Latitude 2	Altitude 3	East Velocity 4	North Velocity 5	Vertical Velocity 6	East Attitude 7	North Attitude 8	Vertical Attitude 9
1	19	54	110	6	67	1	98	89	101
2	14	41	70	4	41	1	97	86	101
3	8	55	94	32	102	2	96	83	101
4	6	14	69	53	71	2	93	77	101
5	10	9	34	9	0.18	1.7	89	77	101
6	6	15	17	29	51	1.3	86	74	101
7	3.8	8.8	15	8.3	5.2	1.5	84	69	101
8	2.6	7.9	7.4	9.1	14.4	1.6	81	67	101
9	3.2	0.6	6.7	26	29	1.7	78	63	101
10	5.9	6.4	0.117	36	39	2.2	73	60	101
11	5.6	5.3	6.5	11	11	2.9	69	60	101
12	7.4	11.6	17	47	48	2.6	66	55	102
13	8.9	13.4	25	17	19	2.7	61	55	102
14	8.9	14	29	10	12	2	57	53	102
15	9	15	29	14	16	1.5	54	51	102
16	9.2	15.5	28.7	13.8	15.1	2.2	50	48	102
17	9.3	15	25	12	13	0.73	48	47	102
18	9.4	16	19	14	14	1.0	46	45	102
19	5	12	18	8	3	3	37	34	103
20	5	12	27	18	15	4	37	30	103